www.nature.com/cr
www.cell-research.com

ARTICLE

Regulators of tubulin polyglutamylation control nuclear shape and cilium disassembly by balancing microtubule and actin assembly

Lei Wang[1]✉, Sharad C. Paudyal[2], Yuchen Kang[1], Mikito Owa[1], Feng-Xia Liang[3], Alexander Spektor[2], Holger Knaut[4], Irma Sánchez[1] and Brian D. Dynlacht[1]✉

Cytoskeletal networks play an important role in regulating nuclear morphology and ciliogenesis. However, the role of microtubule (MT) post-translational modifications in nuclear shape regulation and cilium disassembly has not been explored. Here we identified a novel regulator of the tubulin polyglutamylase complex (TPGC), C11ORF49/CSTPP1, that regulates cytoskeletal organization, nuclear shape, and cilium disassembly. Mechanistically, loss of C11ORF49/CSTPP1 impacts the assembly and stability of the TPGC, which modulates long-chain polyglutamylation levels on microtubules (MTs) and thereby balances the binding of MT-associated proteins and actin nucleators. As a result, loss of TPGC leads to aberrant, enhanced assembly of MTs that penetrate the nucleus, which in turn leads to defects in nuclear shape, and disorganization of cytoplasmic actin that disrupts the YAP/TAZ pathway and cilium disassembly. Further, we showed that C11ORF49/CSTPP1-TPGC plays mechanistically distinct roles in the regulation of nuclear shape and cilium disassembly. Remarkably, disruption of C11ORF49/CSTPP1-TPGC also leads to developmental defects in vivo. Our findings point to an unanticipated nexus that links tubulin polyglutamylation with nuclear shape and ciliogenesis.

Cell Research (2022) 32:190–209; https://doi.org/10.1038/s41422-021-00584-9

INTRODUCTION

Dynamic changes in nuclear shape are frequently observed both in normal cellular processes, including cell migration, proliferation, and differentiation, and in disease states.[1,2] Lobulation is a specific type of nuclear dysmorphia characterized by multi-lobed nuclei with a flower-like, segmented pattern. Lobulation is observed in certain normal hematopoietic cells,[3] such as granulocytes, and in diseases such as laminopathies and cancer,[4,5] although the underlying regulatory mechanisms and functional consequences are not completely understood. It is known that nuclear shape is tightly regulated by mechanical forces generated through interactions between actin and microtubule (MT) networks and nesprin and SUN proteins, which comprise the Linkers of the Nucleoskeleton and Cytoskeleton (LINC) complex within the nuclear envelope.[6] Previous studies showed that MT depolymerization with nocodazole or treatment with a tubulin acetyltransferase (Nat10) inhibitor significantly reduced nuclear lobulation in mature neutrophils and laminopathic cells, respectively, indicating a direct role for MT organization in nuclear lobulation.[7,8] However, it is still not known how MT assembly and organization are regulated to suppress nuclear lobulation.

It is known that MT assembly, stability, and function are regulated by tubulin post-translational modifications (PTMs), including acetylation, methylation, phosphorylation, polyglutamylation, polyglycylation, and tyrosination.[9] These modifications are maintained by tubulin-modifying enzymes and serve to regulate the binding of microtubule-associated proteins (MAPs), a group that includes molecular motors and proteins that regulate MT dynamics and cleavage.[10] Dysregulation of microtubular PTMs has been linked to a wide array of diseases, including neuronal, blood, and muscle disorders, ciliopathies, and cancer.[11] Tubulin polyglutamylation levels are maintained by the tubulin glutamylase family of tubulin tyrosine ligase-like (TTLL) proteins and the cytosolic carboxypeptidases (CCPs), a family of tubulin deglutamylases. Tubulin polyglutamylase complex (TPGC) was the first protein complex identified with tubulin polyglutamylase activity.[12,13] TPGC is comprised of a catalytic subunit, tubulin tyrosine ligase-like 1 (TTLL1), and four additional subunits, tubulin polyglutamylase complex subunits 1 and 2 (TPGS1 and TPGS2), leucine rich repeat containing 49 (LRRC49), and nicolin 1 (NICN1).[12] Previous studies showed that TTLL1 is not active as a monomer, suggesting a regulatory role for the associated TPGC subunits, although their functions are currently unknown.[12,14] Depletion of TTLL1 or TPGS1 leads to decreased tubulin polyglutamylation levels and impairs the binding of a group of MAPs, including KIF1A, KIF5, cytoplasmic dynein, and MAP1A in neurons.[12,15] Characterization of *TTLL1* and *TPGS1* knockout mice demonstrated that these proteins are required for vesicle

[1]Department of Pathology, New York University Cancer Institute, New York University School of Medicine, New York, NY, USA. [2]Department of Radiation Oncology, Dana-Farber Cancer Institute, Brigham and Women's Hospital, Harvard Medical School, Boston, MA, USA. [3]Microscopy Laboratory, Division of Advanced Research Technologies, NYU Langone Health, New York, NY, USA. [4]Skirball Institute of Biomolecular Medicine, New York University School of Medicine, New York, NY, USA. ✉email: Lei.Wang@nyulangone.org; Brian.Dynlacht@nyulangone.org

Received: 24 March 2021 Accepted: 5 October 2021
Published online: 15 November 2021

transport and synaptic function, maintenance of body fat equilibrium, and the development of airway cilia and sperm flagella.[15–18] Recent studies suggest that MT-associated proteins are also involved in MT–actin cross-linking, and MAPs can serve as MT–actin cross-linkers by directly binding to both MT and actin.[10] Likewise, Septins can coordinate actin and MT remodeling by binding both MT and actin.[19,20] Moreover, actin nucleators such as profilins and formins, which promote actin assembly by enhancing activation of the N-WASP–ARP2/3 complex, can also bind MT.[21,22] Despite these advances, it is still unknown whether the TPGC and tubulin modifications, such as polyglutamylation, coordinate MT–actin interactions and actin organization and thus exert broader functional roles in regulating nuclear morphology and ciliogenesis.

Primary cilia are MT-based, antenna-like projections found at the surface of most eukaryotic cells that have ceased proliferation.[23] Cilia sense extracellular stimuli and are assembled from centrioles that have formed basal bodies.[24,25] MT within the ciliary axoneme are also subject to PTMs, which play important roles in regulating ciliogenesis and ciliary signaling.[26–28] Thus far, a number of TTLLs and CCPs, including TTLL1, TTLL5, TTLL6, TTLL9, CCP1 and CCP5, have been shown to coordinate ciliary axonemal polyglutamylation.[28] However, the effect of axoneme polyglutamylation on ciliogenesis remains elusive, partially owing to tissue- and species-specific roles and a lack of mechanistic insights. For example, depletion of TTLL1 in mice led to shortened sperm flagella but normal respiratory cilia, whereas depletion of TTLL1 in *Tetrahymena* did not affect cilia formation.[12,17,18,28] In addition, depletion of TTLL5 in the human RPE1 cell line did not affect cilium length but instead promoted cilium disassembly,[26] while depletion of TTLL9 in *Chlamydomonas* led to elongated flagella and suppression of ciliary disassembly.[29] Beyond such species-, tissue-, and cilia type-specificity, these data also suggest that the regulatory impact of individual TTLLs on ciliogenesis could depend on substrate preferences, and specific TTLL family members could exhibit overlapping and distinct activities. More importantly, it remains unknown if PTM of cytoplasmic MT also plays an important role in regulating ciliogenesis.

Assembly of primary cilia is a complex process that requires intraflagellar transport (IFT) within the organelle and transport of cargoes on centriolar satellites (CSs), peri-centrosomal, electron-dense granules that are transported by MT to dynamically regulate the composition of centrosomes.[30,31] Depletion of CS proteins can disrupt MT anchoring to centrosomes,[32–36] and recent proteomic data also indicate a close relationship between MAPs and CSs, suggesting that CSs could play an important role in regulating MT dynamics.[37,38] However, whether CSs are able to regulate MT assembly, stability, and PTM, and whether they affect nuclear shape or cilium disassembly have not been explored.

Although considerable progress has been made in understanding the biological role of tubulin polyglutamylation and the underlying enzymatic machinery needed to deposit this PTM, it is not known about how TPGC assembly and activity are regulated and whether this enzyme plays a role, if any, in regulating cytoskeletal organization. Furthermore, apart from components of the nuclear envelope and the associated LINC complex, cytoplasmic regulators of nuclear shape have not been comprehensively identified. In this study, through a combination of proteomics, cell-based functional studies, and the use of an animal model, we identified and characterized a novel regulator of TPGC, C11ORF49, that regulates both nuclear lobulation and cilium disassembly. Mechanistically, C11ORF49 regulates the assembly and stability of the TPGC and thereby modulates polyglutamylation of MT, which antagonizes MAP4 binding. Loss of C11ORF49 dramatically enhances the recruitment of MAP4 to MTs, which in turn promotes MT nucleation and polymerization and nuclear lobulation by promoting assembly of MT that penetrate the nucleus. Importantly, we found that loss of C11ORF49 or TPGC subunits also impairs MT association of actin nucleators and MT–actin crosslinkers, perturbing actin organization, provoking cytoplasmic retention of the co-activator Yes Associated Protein (YAP), and blocking the expression and the recruitment of cilium disassembly regulators. Interestingly, we showed that the functional role of C11ORF49 in cilium disassembly could be distinguished mechanistically from its role in nuclear shape control. These alterations lead to persistent ciliation during the cell cycle and developmental defects. Based on the observations in this study, we propose that C11ORF49 and LRRC49, which we have re-named centriolar satellite-associated tubulin polyglutamylation proteins, CSTPP1 and CSTPP2, respectively, are novel cytoplasmic regulators of both cilium disassembly and nuclear morphology.

RESULTS

C11ORF49/CSTPP1 knockout results in defects in nuclear shape, ciliogenesis, and cytoskeleton organization

We previously identified two centrosomal proteins, Talpid3 and C2CD3, as regulators of centrosome maturation and ciliogenesis.[39] To understand the mechanisms behind their regulatory roles, we performed a proteomic screen for Talpid3- and C2CD3-binding partners using a proximity labeling (Bio-ID) approach.[40] Here, each protein was tagged with the BirA ligase, and proteins that were biotinylated within proximity of each protein were purified via binding to avidin and subjected to mass spectrometric sequencing. Among the positive hits, we identified C11ORF49/CSTPP1, a CS protein of unknown function[38] (Supplementary information, Fig. S1).

C11ORF49/CSTPP1 is evolutionarily conserved among vertebrates, and the human *C11ORF49/CSTPP1* gene encodes a 337-amino-acid protein lacking any recognizable protein domains. To gain insight into the function of C11ORF49/CSTPP1, we used CRISPR/Cas9-mediated gene editing to generate a *C11ORF49/CSTPP1*$^{-/-}$ retinal pigment epithelial (RPE1) cell line (clone #1) (Supplementary information, Fig. S2a), since RPE1 cells are an established in vitro model for studying primary cilia. First, we visualized the assembly of cilia, organization of CSs, and cytoskeletal organization by immunofluorescence (IF). Remarkably, we found that ~60% of *C11ORF49/CSTPP1* KO cells possessed a multi-lobed nucleus (Fig. 1a), commonly found only in laminopathies, cancers, and certain normal hematopoietic cells. The impact on nuclear dysmorphia in *C11ORF49/CSTPP1* KO cells matched that observed with the ablation of LINC proteins (nesprins1/2) and Lamin A/C, known to control nuclear shape.[7,41]

Moreover, although primary cilia normally assemble in quiescent cells, we observed a significant increase in the population of ciliated, growing *C11ORF49/CSTPP1* KO cells. We confirmed that both phenotypes were specific by generating a second *C11ORF49/CSTPP1* KO clone (clone #5) and by reintroducing a cDNA encoding C11ORF49/CSTPP1 into *C11ORF49/CSTPP1* KO cells, which rescued both nuclear lobulation and abnormal ciliation (Supplementary information, Figs. S2a, b and S3a). Since both clones exhibited the same phenotypes, *C11ORF49/CSTPP1* KO clone #1 was used in all subsequent studies. In contrast with the loss of C11ORF49/CSTPP1, overexpression of this protein did not impair ciliogenesis or nuclear shape (Supplementary information, Fig. S2c).

In addition, we found that *C11ORF49/CSTPP1* KO cells exhibited markedly reduced F-actin staining, suggesting that the actin network was re-organized (Fig. 1a and see below). On the other hand, the organization of MT networks appeared grossly normal in interphase *C11ORF49/CSTPP1* KO cells (Supplementary information, Fig. S3b). Given the important role of MT in regulating nuclear lobulation, we next examined MT assembly in these cells using MT re-growth assays. By quantifying the intensity of MT nucleated from centrosomes, we observed markedly enhanced

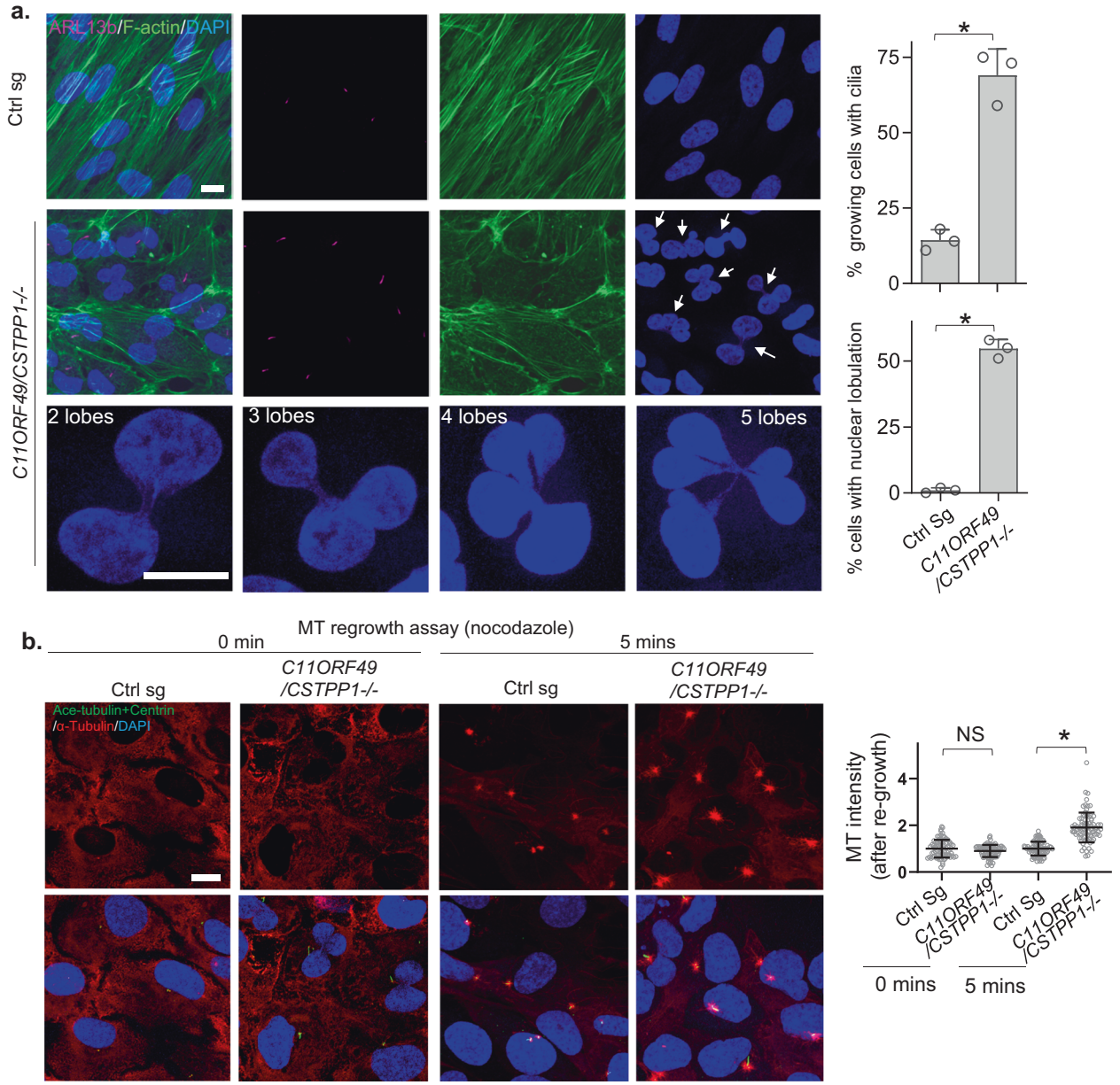

Fig. 1 C11ORF49/CSTPP1 regulates ciliogenesis, nuclear shape, and cytoskeletal dynamics. a Ciliogenesis, nuclear shape, and actin organization were examined in cycling control and *C11ORF49/CSTPP1*$^{-/-}$ cells by IF using indicated antibodies. Arrows indicate cells with multi-lobed nuclei. Representative examples of *C11ORF49/CSTPP1*$^{-/-}$ cells with 2–5 nuclear lobes are shown at bottom. Nuclei with 2 or more lobes were defined as lobulated or multi-lobed. **b** MT organization in control and *C11ORF49/CSTPP1*$^{-/-}$ cells was examined after MT de-polymerization (0 min, after 1 h treatment with 10 μM nocodazole) and re-growth (5 min after removal of nocodazole) by IF using indicated antibodies. Intensity of MT asters was quantified. To rule out contributions of MT signal from cilia, we quantified MT signal in cells without cilia (thus cilia are not a confounding factor in this experiment). Statistical analyses of three independent experiments are presented as means ± SD. *$P < 0.05$ (unpaired *t*-test). For each group, a minimum of 100 cells/experiment was averaged, except for **b**, the sample number for which is 80 cells/experiment. Scale bars, 10 μm.

MT nucleation and re-growth in *C11ORF49/CSTPP1* KO cells after de-polymerization with nocodazole (Fig. 1b) or cold treatment (Supplementary information, Fig. S3c), as compared to WT cells. We further confirmed that MT growth velocity was enhanced in *C11ORF49/CSTPP1* KO cells by dynamically tracking GFP-tagged EB1, a MT plus-end binding protein, in living cells and quantitating MT growth speed (Supplementary information, Fig. S3d). Since C11ORF49/CSTPP1 localizes to CSs,[38] which traffic along MTs, we also examined CS appearance in cells lacking this protein. We stained *C11ORF49/CSTPP1* KO cells with a canonical CS marker, PCM1, and found that the absence of C11ORF49/CSTPP1 did not detectably impact CS organization (Supplementary information, Fig. S3b). Taken together, our data suggest that C11ORF49/CSTPP1 is a multi-functional protein with important roles in regulating nuclear shape, ciliogenesis, and cytoskeleton dynamics.

C11ORF49/CSTPP1 regulates the stability of tubulin polyglutamylase complex

To study how loss of C11ORF49/CSTPP1 leads to the diverse set of phenotypes described above, we re-examined our BioID data to search for additional proteins captured within the neighborhood of Talpid3 and C2CD3. Interestingly, among this group, we also found two subunits of the TPGC, LRRC49/CSTPP2 and TPGS1 (Supplementary information, Fig. S1). TPGC was first identified in

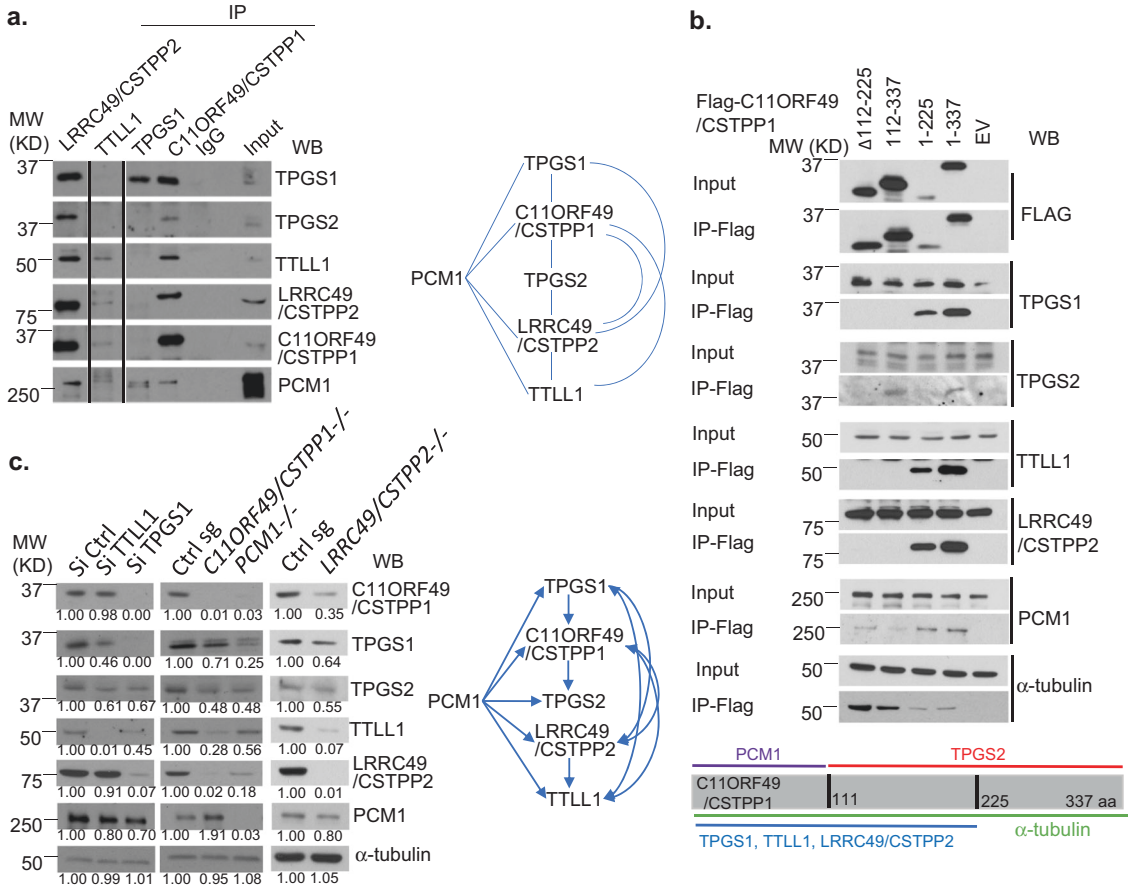

Fig. 2 C11ORF49/CSTPP1 interacts with, and regulates, the stability of tubulin polyglutamylase complex (TPGC). a Western blotting assay of endogenous proteins after immunoprecipitation of HEK293T cell extracts with antibodies indicated at the top of panel. Right, Summary of potential protein–protein interactions. Each line represents co-precipitated proteins. **b** HEK293T cells were transfected with plasmids corresponding to the empty vector (EV) or the indicated Flag-C11ORF49/CSTPP1 fragments for 48 h, and lysates subjected to immunoprecipitation with anti-Flag antibody. The inputs and the immunoprecipitates were analyzed by western blotting assay with the indicated antibodies. Bottom, schematic representation of protein–protein interaction domains in C11ORF49/CSTPP1 based on immunoprecipitation data. **c** TPGC and other CS proteins were examined in lysates from controls and cells depleted of indicated proteins by western blotting using indicated antibodies. Numbers at the bottom of each lane represent the quantification of band intensities, which was first normalized to the band in controls and then normalized to the intensities of each corresponding α-tubulin band. Right, summary of hierarchical regulation of CS and TPGC protein levels.

brain extracts as a regulator of MT polyglutamylation.[12,13] Recently, LRRC49/CSTPP2 and TPGS1 were reported to localize to CS.[37,38] Since we observed aberrant MT assembly in *C11ORF49/CSTPP1* KO cells (Fig. 1b), and dysregulation of MT-generated mechanical forces is thought to play a role in promoting nuclear lobulation,[7,8] we hypothesized that C11ORF49/CSTPP1 could functionally interact with TPGC on CS to regulate MT assembly and prevent nuclear lobulation. Therefore, we examined interactions between C11ORF49/CSTPP1 and TPGC subunits by immunoprecipitation (Fig. 2a). We found that C11ORF49/CSTPP1 co-precipitated with four subunits of TPGC, although we were unable to detect NICN1 owing to the lack of suitable antibodies. Reciprocal immunoprecipitations with LRRC49/CSTPP2 and TTLL1 antibodies confirmed their interaction with C11ORF49/CSTPP1. We also found that C11ORF49/CSTPP1 and other TPGC subunits that we tested associated with PCM1, further indicating that C11ORF49/CSTPP1 and TPGC could be transported on CS (Fig. 2a). To identify the domains of C11ORF49/CSTPP1 required to interact with TPGC subunits and PCM1, we performed immunoprecipitation experiments after expressing full-length C11ORF49/CSTPP1 and several truncations in HEK293T cells. We found that C11ORF49/CSTPP1 interacted with TPGS1, LRRC49/CSTPP2, and TTLL1 through residues 1–225, whereas robust interactions between C11ORF49/CSTPP1 and TPGS2 or PCM1 required residues 112–377 or 1–111, respectively (Fig. 2b). Moreover, each of the C11ORF49/CSTPP1 truncations was able to interact with α-tubulin, albeit to varying degrees, suggesting multiple regions of contact (Fig. 2b).

Next, we examined the levels of TPGC subunits in *C11ORF49/CSTPP1* KO cells and found a significant decrease in LRRC49/CSTPP2, TTLL1, and TPGS2 protein levels, confirming that C11ORF49/CSTPP1 plays an essential role in the assembly and/or stability of TPGC (Fig. 2c). Using CRISPR/Cas9-based gene editing, we generated *LRRC49/CSTPP2* KO cells, since this protein interacts with other TPGC subunits (Fig. 2). Interestingly, we also observed markedly decreased levels of TPGC subunits and C11ORF49/CSTPP1 in *LRRC49/CSTPP2* KO cells. Moreover, we observed a significant decrease in the levels of C11ORF49/CSTPP1 and TPGC subunits in *PCM1* KO cells (Fig. 2c), demonstrating that CSs play a critical role in the assembly and/or stability of TPGC. Collectively, these data suggest that (1) C11ORF49/CSTPP1 is a bona fide novel regulator of TPGC and (2) both C11ORF49/CSTPP1 and LRRC49/CSTPP2 play key roles in regulating the assembly, stability, and function of TPGC.

C11ORF49/CSTPP1 and TPGC subunits coordinately regulate nuclear lobulation, ciliogenesis, and cytoskeleton organization

We further investigated the incorporation of C11ORF49/CSTPP1 into the TPGC by examining the recruitment of the complex to CSs after depleting several components with siRNAs. We found that PCM1 recruits TPGS1 to satellites, and TPGS1 was required to recruit C11ORF49/CSTPP1 and LRRC49/CSTPP2. CS localization of C11ORF49/CSTPP1 and LRRC49/CSTPP2 was co-dependent, while neither protein was required to recruit either PCM1 or TPGS1 (Fig. 3a). Since three existing commercial and in-house sources of antibodies were unable to detect the localization of endogenous C11ORF49/CSTPP1, we generated a cell line in which the Flag epitope was introduced into the native *C11ORF49/CSTPP1* locus using gene editing in RPE1 cells. We confirmed that the knock-in Flag-tagged protein was expressed at levels indistinguishable from the endogenous protein (Supplementary information, Fig. S4a). Importantly, use of this knock-in cell line confirmed the CS localization of C11ORF49/CSTPP1 (Supplementary information, Fig. S4a). Moreover, we found that C11ORF49/CSTPP1 was widely distributed through the cytoplasm (Supplementary information, Fig. S4b), near the cell periphery, and at a distance from centrosomes. High resolution imaging showed that, similar to PCM1 and other CS proteins, a large number of C11ORF49/CSTPP1 foci pervasively localized along MTs (Supplementary information, Fig. S4b), consistent with the observed interaction between C11ORF49/CSTPP1 and α-tubulin (Fig. 2b) and previous reports that CS travel along MTs. The interaction between C11ORF49/CSTPP1 and MTs was further tested using a cell-free assay in which we produced C11ORF49/CSTPP1 in mammalian cells, purified the protein, and examined its ability to bind MT assembled in vitro. We observed robust binding of C11ORF49/CSTPP1 to MT (Fig. 3b). These data indicate that C11ORF49/CSTPP1 might regulate the tubulin polyglutamylation activity of TPGC by modulating the binding/trafficking of the complex along MT. To examine whether C11ORF49/CSTPP1 and LRRC49/CSTPP2 localize to centrosomes as well as satellites, we dispersed CS (which depend on the integrity of MT) using nocodazole and found that these proteins do not stably localize on centrosomes (Fig. 3c). We were unable to observe CS or any specific staining of TPGS2, TTLL1, or NICN1 after ectopic expression of amino- or carboxy-terminal fusion proteins (Supplementary information, Fig. S4c), suggesting that for proper localization, they may be dependent on other components that could be limiting or that these proteins could dynamically localize at both CS and alternate locations. Taken together, with our data suggesting biochemical interactions between C11ORF49/CSTPP1, TPGC, and PCM1, we conclude that TPGC and C11ORF49/CSTPP1 are hierarchically assembled into complexes transported on MT.

Given that C11ORF49/CSTPP1 regulates the assembly and stability of TPGC, we asked whether disruption of other TPGC subunits leads to phenotypes similar to those observed in *C11ORF49/CSTPP1* KO cells. Importantly, proliferating *LRRC49/CSTPP2* KO cells also displayed dramatically increased levels of ciliation and nuclear lobulation, although the degree of lobulation was somewhat lower than that of *C11ORF49/CSTPP1* KO cells (Fig. 3d). To test the generality of these observations, we depleted TPGS1 and TTLL1 in RPE1 cells, and interestingly, we observed increased ciliogenesis but no impact on nuclear shape (Fig. 3d). We also examined ciliogenesis, MT assembly, actin organization, and nuclear lobulation in *PCM1* KO cells. Ciliogenesis was blocked in *PCM1* KO cells, consistent with prior studies,[42–44] indicating a dominant role for PCM1 in cilium assembly. Like C11ORF49/CSTPP1 ablation, depletion of TPGS1, TTLL1, LRRC49/CSTPP2, and PCM1 also led to enhanced MT re-growth after de-polymerization (Supplementary information, Fig. S5a). Depletion of TPGS1, TTLL1, LRRC49/CSTPP2, but not PCM1, led to reduced F-actin staining (Supplementary information, Fig. S5b). Interestingly, nuclear morphology was normal in *PCM1* KO cells, although the localization and levels of TPGC subunits were significantly impaired in these cells, implying that the loss of other CS proteins in *PCM1* KO cells could counter-balance the impact of ablating C11ORF49/CSTPP1 and LRRC49/CSTPP2 on nuclear shape. This conclusion is supported by the fact that ~65 proteins have been reported to localize on CS — many of which require PCM1 for CS localization and maintenance of protein stability and function — and hundreds of proteins were found in close association with CS in recent proteomic studies.[31]

Taken together, these data demonstrate that TPGC localizes to CS and MTs and plays an important role in regulating ciliogenesis, cytoskeleton organization, and nuclear lobulation, but there may be subunit-specific functions for C11ORF49/CSTPP1 and LRRC49/CSTPP2 that govern nuclear shape (see Discussion).

Tubulin polyglutamylation antagonizes binding of microtubule-associated proteins (MAPs) and promotes association of actin nucleators

To mechanistically understand how TPGC regulates cytoskeletal organization, we focused on TTLL1, the enzymatic subunit of TPGC.[12] TTLL1 is a polyglutamylase, catalyzing the modification of MT and other substrates. Polyglutamylation of MT regulates the binding of microtubule-associated proteins (MAPs), which in turn regulate MT structure, dynamics, and function.[10] MAPs also serve as MT–actin crosslinkers by directly binding to both MT and actin[10] Likewise, polyglutamylation of MT regulates the binding of septins, which coordinate actin and MT remodeling by binding both MT and actin[19,20] Recent studies suggest that actin nucleators like profilins and formins, which promote actin assembly by enhancing activation of the N-WASP–ARP2/3 complex, can also bind MT.[21,22] We therefore reasoned that TPGC-mediated MT polyglutamylation could regulate MT/actin organization by modulating the binding or recruitment of MAPs, actin nucleators, and MT–actin crosslinkers to MT. We examined the degree to which representative proteins (MAP1S, MAP4, SEPTIN2, PROFILIN1, ARP2, N-WASP) were enriched in the polymerized microtubule fraction (MT-fraction) vs the total cytosolic fraction (Cyto-fraction)[20] of cells depleted of C11ORF49/CSTPP1 and TTLL1. Notably, we observed decreased polyglutamylated tubulin (poly-E) levels in the polymerized MT fraction, as well as a reduced association of PROFILIN1, N-WASP and ARP2 with polymerized MT in cells depleted of C11ORF49/CSTPP1 or TTLL1 (Fig. 3e). In striking contrast, we observed enhanced association of MAP1S and MAP4 with polymerized MTs in depleted cells, suggesting that MT polyglutamylation levels could modulate the binding of MAPs and actin nucleators in an antagonistic manner. We noted that altered levels of these proteins were observed specifically in the MT-fraction but not in the cytosolic fraction of cell lysates (Fig. 3e). Importantly, this demonstrates that TPGC specifically regulates the recruitment, but not the overall abundance, of these cytoskeletal regulatory proteins and that TPGC primarily regulates poly-E levels of polymerized MT. Overall, these data suggest that TPGC-mediated tubulin polyglutamylation could balance both MT and actin assembly by modulating binding and/or association of MAPs and actin nucleators with MT.

Loss of C11ORF49/CSTPP1 promotes the formation of MTs that penetrate the nucleus, resulting in nuclear lobulation

To understand how nuclear shape is regulated by TPGC, we tracked the formation of nuclei during mitosis in *C11ORF49/CSTPP1* KO cells by live-cell imaging of MT and nuclei with GFP-tubulin and H2B-mRuby2, respectively. We found that mitotic progression was generally normal in *C11ORF49/CSTPP1* KO cells, with no increased incidence of multipolar spindles, lagging or bridging chromosomes, or micronuclei (Supplementary information, Fig. S6a). However, lobulated nuclei appeared in late telophase in *C11ORF49/CSTPP1* KO cells, preceded by the

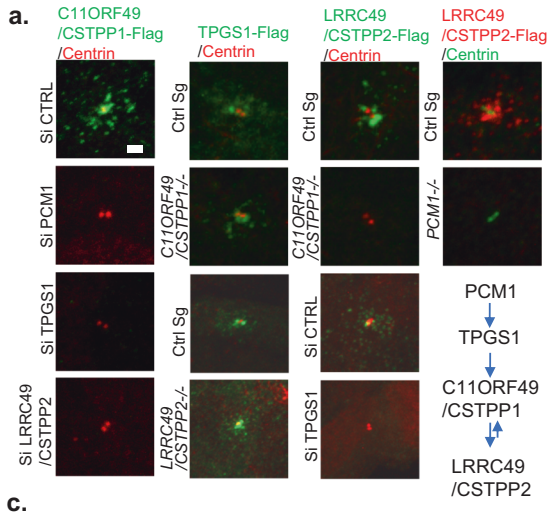

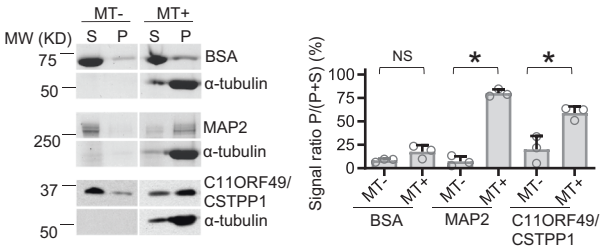

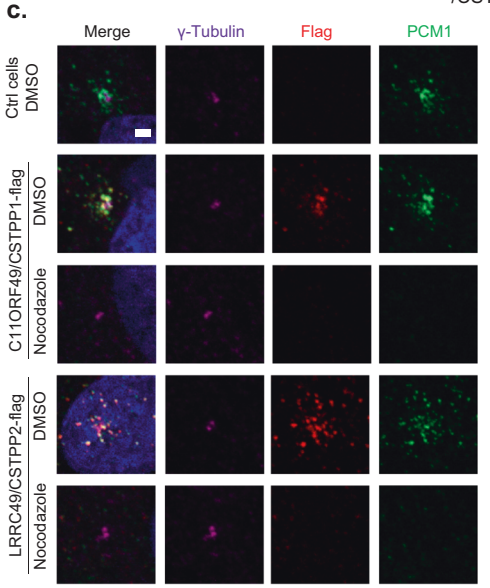

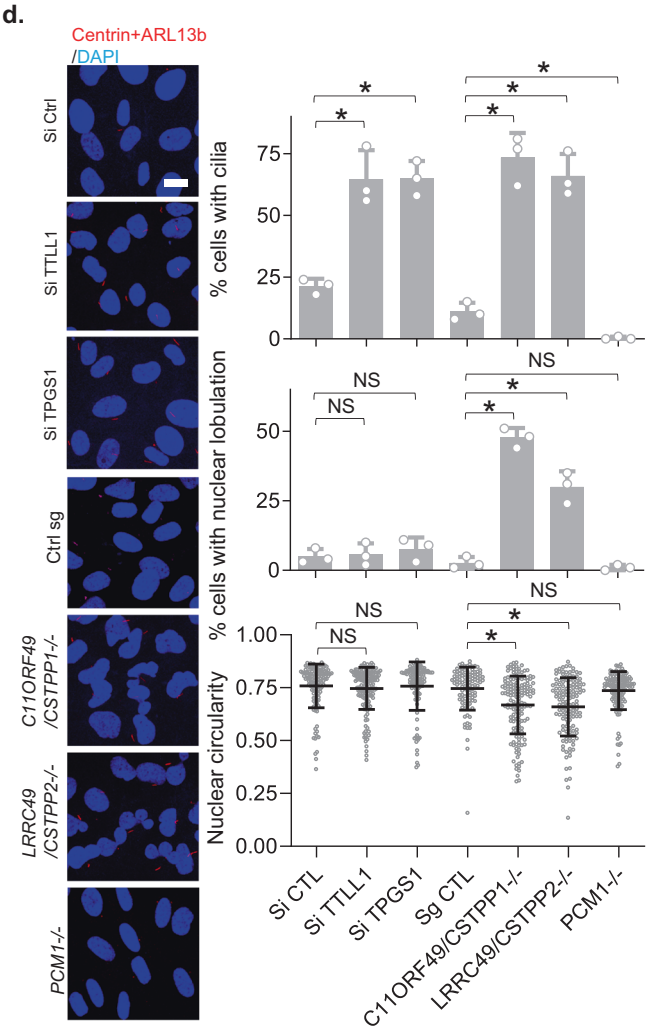

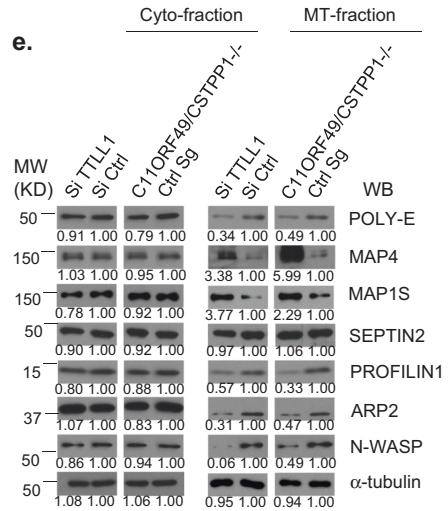

appearance of MT that penetrated the nucleus at the boundaries of prospective nuclear lobes (Fig. 4a). Importantly, we found that the MTs penetrating the nucleus were observed in KO cells after completion of chromosome separation during anaphase and prior to completion of nuclear envelope re-assembly. Immunofluorescent staining of fixed *C11ORF49/CSTPP1* KO cells confirmed the presence of MTs penetrating the nucleus in telophase and indicated that they originate from centrosomes (Fig. 4b). We further characterized the relationship between these aberrant MTs and the nuclear membrane by co-staining MT and

Fig. 3 C11ORF49/CSTPP1 and TPGC assembly on CSs coordinately regulates cytoskeleton organization, ciliogenesis and nuclear lobulation. a Localization of Flag-tagged TPGS1, C11ORF49/CSTPP1, and LRRC49/CSTPP2 was examined in control RPE1 cells, and cells depleted of the indicated proteins with siRNA for 3 days and then visualized with specified antibodies. **b** C11ORF49/CSTPP1 binds to MTs in vitro. MT binding assays were performed using Flag-tagged C11ORF49/CSTPP1 purified from HEK293T cells and BSA or MAP2. Proteins in the supernatant (S) and pellet (P) fractions were visualized by Coomassie blue staining (BSA and MAP2) or western blotting assay (C11ORF49/CSTPP1). **c** RPE1 cells were infected with lentivirus expressing Flag-C11ORF49/CSTPP1 or Flag-LRRC49/CSTPP2 for 3 days and incubated with nocodazole (1 μg/mL) for 8 h. Cells were immuno-stained with α-tubulin (purple), PCM1 (green) and Flag (red). Scale bars, 2 μm in **a**, **b**. **d** Ciliogenesis and nuclear shape were examined in control RPE1 cells and cells depleted of TTLL1, TPGS1, C11ORF49/CSTPP1, LRRC49/CSTPP2, or PCM1 by IF using indicated antibodies. Nuclei with > 2 lobes were defined as lobulated or multi-lobed. Nuclei circularity (form factor) was analyzed by CellProfiler software. **e** MAPs and actin nucleators were examined in cyto- and MT-fractions from controls and cells depleted of indicated proteins by western blotting using indicated antibodies. Numbers at the bottom of each lane represent the quantification of band intensities, which was first normalized to the band in controls and then normalized to the intensities of each corresponding α-tubulin band. Scale bars, 10 μm in **c**. Statistical analyses of three independent experiments are presented as means ± SD. *$P < 0.05$ (unpaired *t*-test or Mann-Whitney test). For each group, a minimum of 100 cells/experiment was averaged.

Lamin B1, a nuclear membrane marker, and using high-resolution microscopy. We found that these MTs can deeply penetrate the nucleus, with a subset transecting the entire nucleus. Further, the MTs penetrating the nucleus are generally associated with the nuclear membrane (Supplementary information, Fig. S6b), suggesting that they could promote formation of multi-lobed nuclei by interrupting or creating tension on the nuclear envelope. The disposition of these aberrant MTs was further confirmed by combining correlative light microscopy with immuno-electron microscopy (CLEM) to detect MTs transversing the NE. Here, we found that MTs were positioned at the boundary of nuclear lobes and sometimes extended into the center of the nucleus, accessing "holes" in the membrane that enveloped the MTs (Fig. 5a and Supplementary information, Fig. S6c).

These data suggest a potential role for assembly of aberrant MTs that penetrate the nucleus and promote formation or maintenance of nuclear lobulation in *C11ORF49/CSTPP1* KO cells. To further test this model, we asked whether disruption of the MT network with nocodazole treatment could rescue the nuclear lobulation observed in *C11ORF49/CSTPP1* KO cells, which we assessed by inspection of nuclear shape and by calculating nuclear circularity. Importantly, we found that MT de-polymerization significantly reduced the extent and frequency of lobulation in these knock-out cells (Fig. 5b). These data strongly suggest that C11ORF49/CSTPP1 suppresses nuclear lobulation, at least in part, by limiting aberrant formation of MTs to penetrate the nucleus and create a multi-lobulated state.

C11ORF49/CSTPP1 suppresses nuclear lobulation by dampening MAP4-mediated MT assembly

To understand mechanistically how TPGC prevents aberrant MT assembly able to promote nuclear lobulation, we focused on MAPs whose recruitment to MT is regulated by TPGC-mediated polyglutamylation (Fig. 3e). MAP4 has been shown to promote MT assembly and stabilization[45,46] and to regulate ciliogenesis and ciliary length.[47,48] MAP4 was also captured in our proteomic screen (Supplementary information, Fig. S1). It is thought that excessive mechanical forces on the nuclear envelope generated by MTs can lead to nuclear lobulation.[6–8] Therefore, we hypothesized that altered TTLL1 levels could adversely impact the binding of MAP4 to MT, resulting in enhanced MT assembly and aberrant nuclear morphology. Indeed, in IF experiments, we observed decreased polyglutamylation levels on MT and increased MAP4 localization to MT in TTLL1-depleted cells (Fig. 6a, b), consistent with our western blot analysis of MAP4 enrichment in the MT-fraction (Fig. 3e). Conversely, we asked whether enhancing MT polyglutamylation levels by targeted expression of TTLL1 could modulate polyglutamylation levels and MAP4 recruitment. Previous studies suggested that overexpression of TTLL1 alone does not result in elevated levels of MT polyglutamylation,[12,14,49] likely due to the lack of a MT binding domain and a requirement for allosteric regulation or substrate targeting by other TPGC subunits. Therefore, we expressed a chimeric protein in which we fused TTLL1 to the MT-targeting domain of MAP4 (MAP4m).[47] Notably, expression of a fusion protein linking MAP4m to wild-type TTLL1, but not an enzymatically inactive mutant (E326G), led to markedly enhanced polyglutamylation and decreased MT binding by endogenous MAP4, detected by IF experiments with antibodies against Poly-E and an epitope in MAP4 beyond the MAP4m domain, respectively (Fig. 6c). These data are consistent with previous reports that TTLL1 requires accessory proteins to bind MT[12,14,49] and confirmed our previous conclusions based on western blot experiments (Fig. 3e) that TTLL1 activity is required to maintain proper levels of cytoplasmic MT polyglutamylation, which negatively affects the binding of MAP4.

Based on our foregoing observations, we tested the possibility that defects in nuclear morphology and MT assembly, as well as aberrant ciliation, in *C11ORF49/CSTPP1* KO cells stemmed from increased MAP4 recruitment caused by TPGC destabilization. Interestingly, we observed decreased levels of polyglutamylation of cytoplasmic MT and increased MAP4 binding in *C11ORF49/CSTPP1* KO cells (Fig. 6a, b), consistent with the diminished expression and/or stability of TPGC subunits in these cells (Fig. 2c). Moreover, we also observed decreased levels of polyglutamylation of MT and increased MAP4 binding in TPGS1-depleted and LRRC49/CSTPP2 and PCM1 KO cells (Fig. 6a, b). Importantly, when we silenced MAP4 expression with an siRNA in *C11ORF49/CSTPP1* KO cells, we found that the enhanced MT nucleation (defined by quantifying the intensity of MT nucleated from centrosomes during MT regrowth) and nuclear lobulation, but not aberrant ciliation, could be substantially rescued (Fig. 7a, b). Given the observed association between aberrant assembly of MT that penetrate the nucleus and formation/maintenance of nuclear lobes at telophase (Figs. 4 and 5), we reasoned that enhanced MAP4 levels and increased MT polymerization could promote the formation of these MT during nuclear envelope resealing, sectoring the nucleus into compartmentalized lobes. To further test this model to explain the nuclear lobulation observed in *C11ORF49/CSTPP1* KO cells, we asked whether expression of the MAP4m–TTLL1 fusion in *C11ORF49/CSTPP1* KO cells could reduce MT nucleation and rescue nuclear lobulation. Indeed, we found that expression of MAP4m–TTLL1 significantly reduced the extent of MT nucleation and frequency of lobulation in these knock-out cells (Fig. 7c and Supplementary information, Fig. S7a), corroborating our model that C11ORF49 regulates nuclear morphology, at least in part, by controlling MT polyglutamylation and MT assembly. Taken together with our depletion studies, these data also suggest that the aberrant ciliation observed in TPGC-deficient cells is not due to dysregulated MAP4 binding.

Previous studies suggested that defects in spastin-mediated MT severing could contribute to the formation of multi-lobed nuclei and that spastin-mediated MT severing is stimulated by polyglutamylation.[50–53] We speculated that TPGC-mediated MT

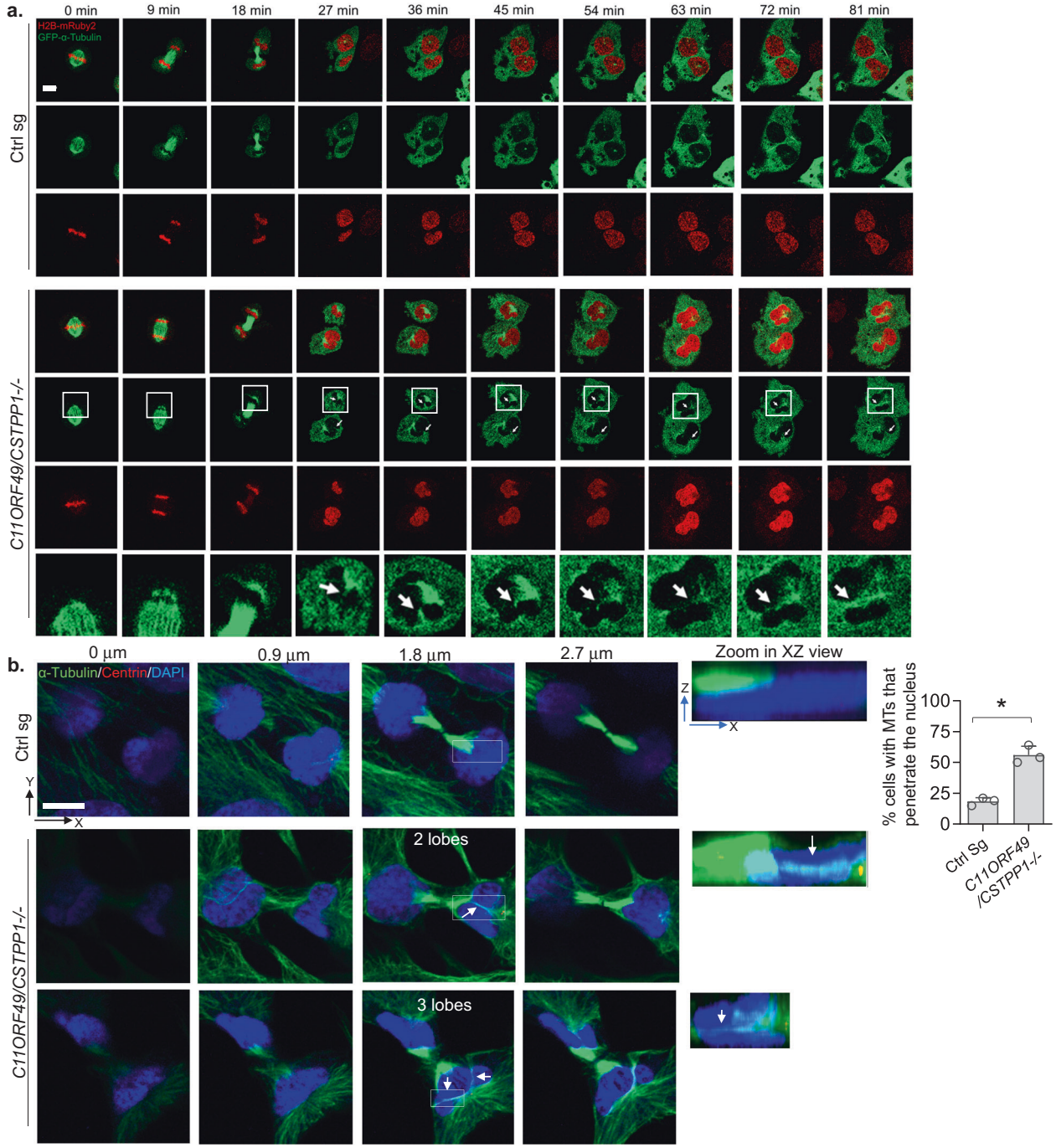

Fig. 4 C11ORF49/CSTPP1 loss promotes assembly of MTs that penetrate the nucleus. a Time-lapse images of control and *C11ORF49/CSTPP1*$^{-/-}$ cells co-expressing GFP-tubulin and H2B-mRuby2. Confocal *z*-stacks were scanned through the entire nucleus at 1-μm intervals. Images of a single *z*-stack of a nucleus with penetrating MTs. Zoomed-in view of nuclear region of each sample of *C11ORF49/CSTPP1*$^{-/-}$ cells is shown at bottom. **b** MT organization was examined in control and *C11ORF49/CSTPP1*$^{-/-}$ telophase cells by IF using indicated antibodies. Arrows indicate MTs penetrating the nucleus. Confocal *z*-stacks were scanned through the entire nucleus at 0.45-μm intervals. The image of a single *z*-stack of a nucleus with MTs penetrating the nucleus and the percentage of cells with these aberrant MTs are shown. Zoomed-in *xz* view of nuclear region of each sample is shown on the right.

polyglutamylation could modulate spastin-mediated MT severing and promote the formation of MTs that penetrate the nucleus. To test this possibility, we first examined the severing of MT in late telophase by quantifying the population of cells with nuclear-penetrating MT after treatment with Spastazoline, a spastin inhibitor (Supplementary information, Fig. S7b). As expected, treatment of control cells with Spastazoline inhibited spastin-mediated MT severing and increased the percentage of cells with MT penetrating the nucleus. Interestingly, the percentage of cells with MT penetrating the nucleus in the untreated *C11ORF49/CSTPP1* KO cell line was comparable to that observed in the Spastazoline-treated control cell line, but treatment of *C11ORF49/CSTPP1* KO cells with Spastazoline did not further augment the percentage of cells with these aberrantly assembled

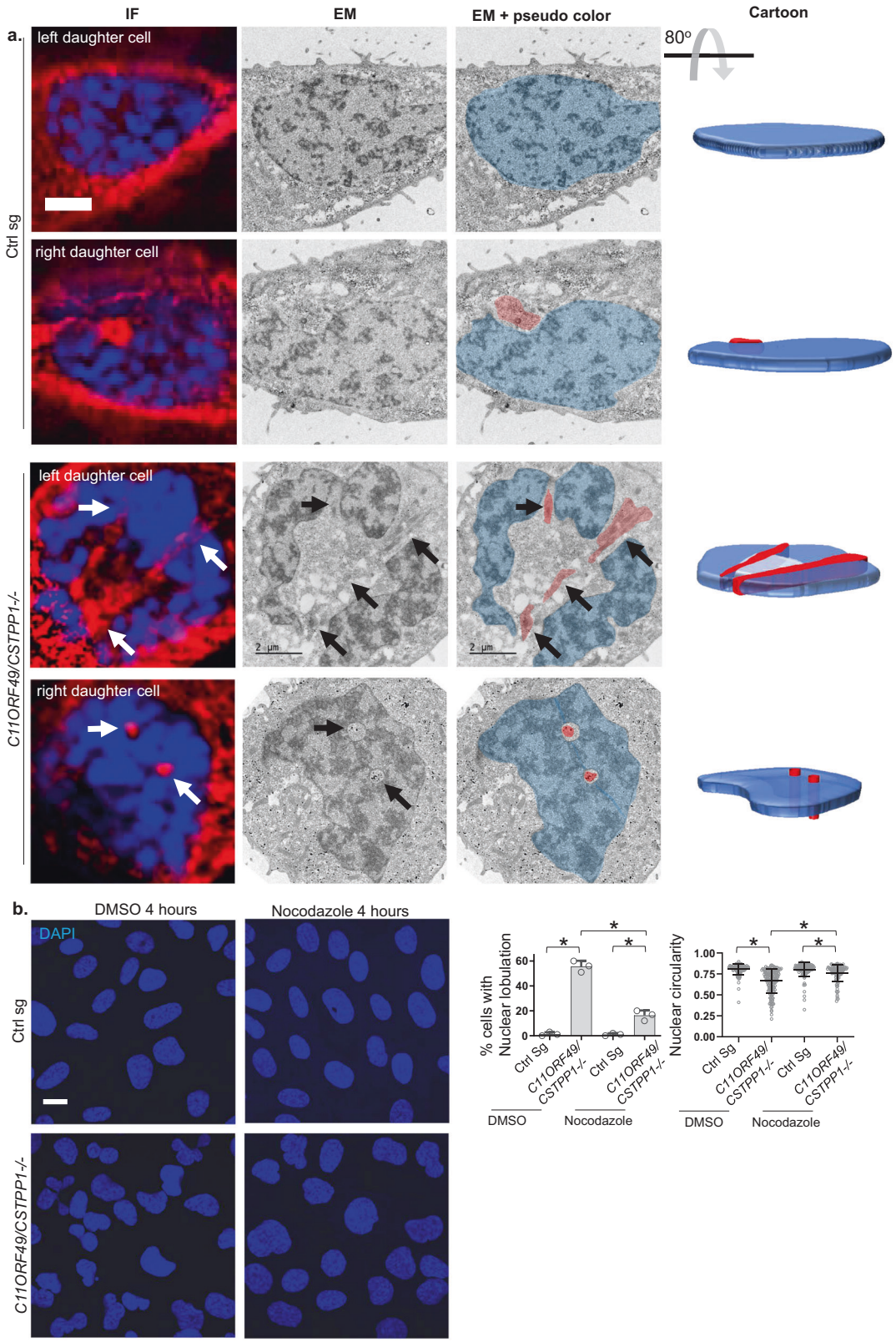

MT. These data suggest that MTs in *C11ORF49/CSTPP1* KO cells are less susceptible to spastin-mediated severing and could contribute to the formation of multi-lobed nuclei. Further, our observations suggest that tubulin polyglutamylation through TPGC functionally collaborates within a spastin-mediated severing pathway. Overall, our data suggest that depletion of C11ORF49/CSTPP1 or other TPGC subunits compromises MT nucleation by abnormally elevating the recruitment of MAP4, which enhances MT assembly and promotes formation of MTs that penetrate the nucleus and distort nuclear shape.

Fig. 5 MTs that penetrate the nucleus in C11ORF49/CSTPP1 KO cells drive lobulation. a MT organization was examined in control and *C11ORF49/CSTPP1*$^{-/-}$ telophase cells using correlative light and electron microscopy (CLEM). IF images and correlative EM images are shown with and without pseudo-color (blue for nucleus, red for MT). Arrows indicate Alexa-546/nano-gold-labeled nuclear-penetrating MTs captured by immuno-EM and conventional microscopy. Schematic of CLEM method used in this study and serial-section EM images of the same nuclei are included in Supplementary information, Fig.S6c. (Right) Cartoons indicate the position of MT based on serial section EM images. Scale bars = 2 μm. **b** Control and *C11ORF49/CSTPP1*$^{-/-}$ RPE1 cells were incubated with nocodazole (10 μM) for 4 h and stained with DAPI to examine nuclear shape. $n \geq 100$ per sample were analyzed in three independent experiments. Nuclei with >2 lobes were defined as lobulated or multi-lobed. $n \geq 40$ per sample were analyzed in three independent experiments in **b**. Circularity of nuclei was measured with CellProfiler software Form factor function. All data are presented as means ± SD. *$P < 0.05$ (unpaired *t*-test or Mann-Whitney test). Scale bars = 10 μm.

Enhanced ciliation in C11ORF49/CSTPP1- and TPGC-deficient cells results from defects in an actin-mediated cilium disassembly pathway

Our foregoing studies pinpointed a mechanistic link between loss of C11ORF49/CSTPP1 and TPGC components and disruption of MT/actin networks. To understand the mechanistic basis for increased ciliation in *C11ORF49/CSTPP1* KO cells and to investigate whether this phenotype could be linked to defects in MT/actin networks, we considered several possibilities. First, we determined whether enhanced ciliation could result from the induction of quiescence through aberrant cell cycle exit. However, FACS analysis showed that the population of G0 cells actually decreased in *C11ORF49/CSTPP1* KO cells (Supplementary information, Fig. S8a), and KO cells continued to cycle, suggesting that enhanced ciliation could not be explained by induction of cell cycle exit. We therefore hypothesized that cilium disassembly could be subverted. RPE1 cells exhibit two "waves" of cilium resorption upon stimulation of serum-starved cells, first, within a few hours after stimulation in G1 phase and then during the G2/M transition.[54] We found that both waves were significantly delayed in KO cells (Fig. 8a). We further examined the extent of ciliation across all cell cycle stages and found an increased frequency of ciliation in G1 and S phase but not G2 or M phase (Supplementary information, Fig. S8b). Moreover, we also observed an increase in cilium length in *C11ORF49/CSTPP1* KO cells before or after serum re-stimulation (Fig. 8a). These data suggest that defects in cilium disassembly contribute to increased ciliation in *C11ORF49/CSTPP1* KO cells. However, several observations suggest that resorption is not abolished altogether, since cell growth is not perturbed, and we do not observe ciliated mitotic cells or centrosome duplication defects, which would result from a permanently ciliated state. We conclude that ablation of C11ORF49/CSTPP1 causes a significant delay in cilium resorption.

It is known that F-actin de-polymerization promotes ciliogenesis while inhibiting cilium disassembly.[55–58] It is also known that centrosomes can act as actin-organizing centers.[59] We showed that loss of C11ORF49/CSTPP1 and TPGC compromises actin organization and the association of actin nucleators and cross-linkers with MT (Fig. 3e and Supplementary information, Fig. S5b). We reasoned that re-organization of actin in *C11ORF49/CSTPP1* KO cells could also contribute to the increased ciliation observed in these cells. WASH is an actin nucleation-promoting factor that activates the actin nucleators, Arp2/3, through its VCA (verprolin homology or WH2-connector-acidic) domain.[60] To test our hypothesis directly, we expressed a GFP-CENTRIN1-VCA[61] fusion protein in *C11ORF49/CSTPP1* KO cells to induce actin filament nucleation at centrosomes. Remarkably, cells expressing the fusion protein exhibited a significant decrease in ciliation as compared to control *C11ORF49/CSTPP1* KO cells expressing GFP-CENTRIN1 only (Fig. 8b). Importantly, and in striking contrast, enforced recruitment of actin nucleators did not alleviate the nuclear lobulation phenotype (Fig. 8b). To further test the contribution of MT-associated actin nucleators to actin/ciliary defects observed in *C11ORF49/CSTPP1* KO cells, we artificially enhanced recruitment of an actin nucleator to MT in *C11ORF49/CSTPP1* KO cells, by fusing the MAP4 MT binding domain to VCA, which enhanced F-actin assembly near MTs and rescued the cilium disassembly defect in *C11ORF49/CSTPP1* KO cells (Fig. 8c, d). Taken together, our data suggest that C11ORF49/CSTPP1 regulates actin assembly by modulating recruitment of actin nucleators to MT, which in turn regulates cilium disassembly.

Mechanistically, de-polymerization of actin filaments has been shown to block nuclear entry of the transcriptional co-activators YAP/TAZ, resulting in decreased expression of PLK1 and Aurora A, which are known to promote cilium disassembly.[62] By examining nuclear staining of YAP, we found that decreased F-actin assembly in *C11ORF49/CSTPP1* KO cells led to cytoplasmic retention of YAP (Fig. 8e). Concordantly, we also observed decreased levels of PLK1 in *C11ORF49/CSTPP1* KO cells (Fig. 8f), suggesting that loss of this protein disables an actin-based YAP-PLK1 cilium disassembly pathway, triggering aberrant ciliation. To further test this hypothesis, we overexpressed a constitutively active YAP mutant (YAP-5SA)[62,63] in growing *C11ORF49/CSTPP1* KO cells to determine if cilium disassembly could be rescued. Indeed, YAP-5SA localized to nuclei and rescued aberrant ciliation in *C11ORF49/CSTPP1* KO cells (Fig. 8g). Together with previous data showing grossly normal cell cycle progression (Supplementary information, Figs. S6a and 8a), we conclude that decreased levels of PLK1 in *C11ORF49/CSTPP1*$^{-/-}$ cells result in delayed cilium disassembly, although it has no overt impact on PLK1-dependent regulation of cell proliferation and mitosis, probably because of different enzymatic thresholds required to effect each process. Remarkably, we also found decreased PLK1 protein levels in cells depleted of TPGS1, TTLL1, and LRRC49/CSTPP2 (Fig. 8f), consistent with decreased actin assembly and increased ciliation in these cells (Fig. 3d and Supplementary information, Fig. S5b).

To test if other cilium disassembly pathways are also affected in *C11ORF49/CSTPP1*$^{-/-}$ cells, we performed a screen to detect the localization of known cilium disassembly regulators in wild-type and *C11ORF49/CSTPP1* KO cells. We examined the centrosomal and ciliary localization of NEK2, KIF24, HDAC6, AURORA A, phospho-TCTEX1, CPAP, KIF2A, KATANIN, and NDE1,[54,56,57,64–67] since each of these proteins has been implicated in regulating the length or removal/resorption of cilia (Supplementary information, Fig. S8c). Among these proteins, only NDE1 showed moderately decreased centrosomal intensity in cells depleted of TTLL1 or C11ORF49/CSTPP1 (Fig. 8h). NDE1 is a centrosomal protein that promotes primary cilium resorption in RPE1 cells and in zebrafish, likely by tethering the dynein light chain protein, LC8, at the basal body.[65] We showed that decreases in NDE1 intensity after depletion of C11ORF49/CSTPP1 and TTLL1 could not be explained by altered protein levels (Supplementary information, Fig. S8d), leading us to conclude that recruitment per se was impacted.

Taken together, these data lead to two major conclusions: first, increased ciliation in TPGC-depleted cells is due, at least in part, to defects in an actin-dependent YAP-PLK1 cilium disassembly pathway and NDE1 recruitment; second, loss of C11ORF49/CSTPP1 impacts ciliation and lobulation through separable and distinct pathways that involve actin and MT network assembly, respectively.

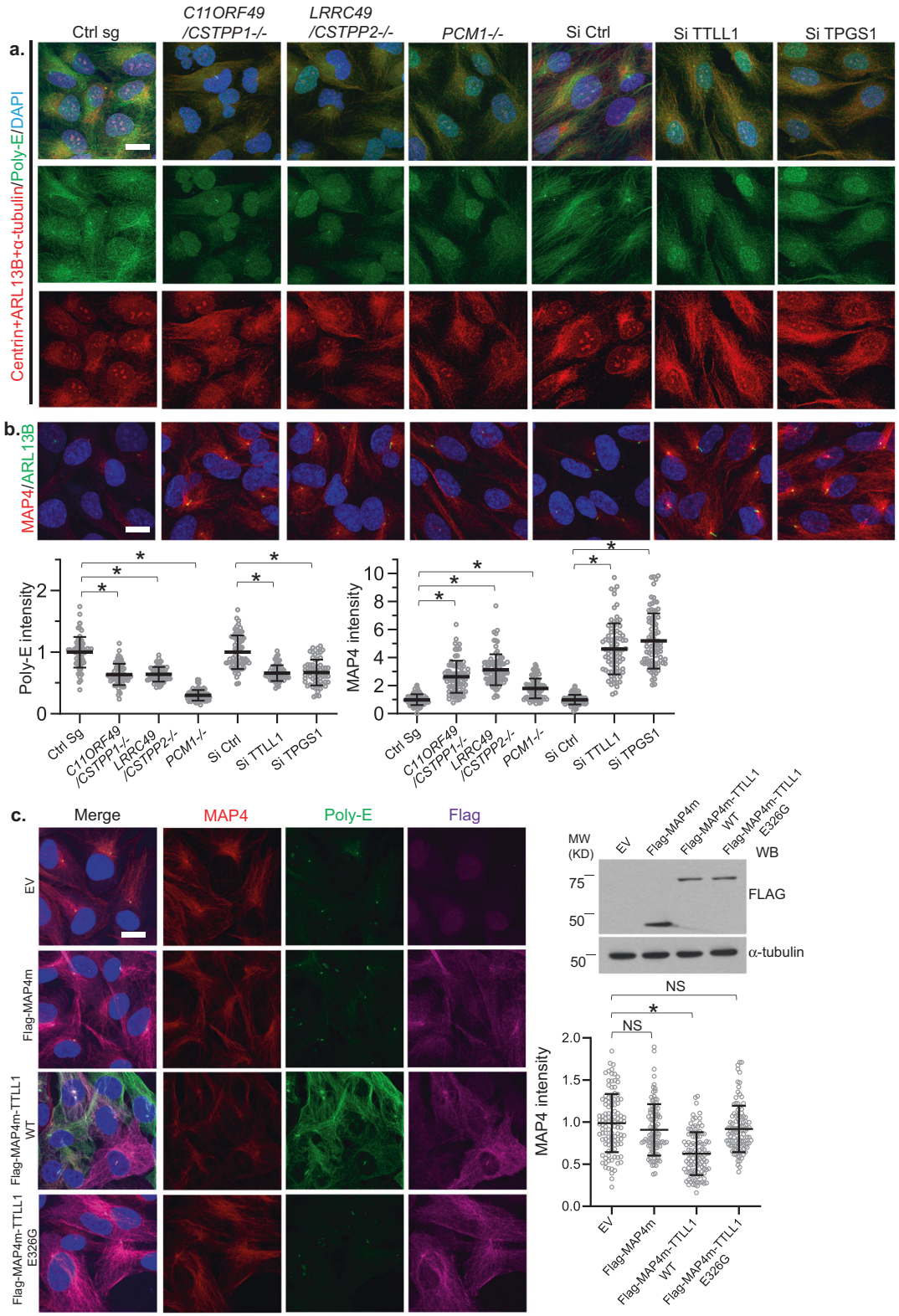

Fig. 6 The C11ORF49/CSTPP1-TPGC axis regulates polyglutamylation of MT and binding of MAP4. a, **b** The intensity of polyglutamylated MT and MAP4 was quantified in control RPE1 cells and cells depleted of TTLL1, TPGS1, C11ORF49/CSTPP1, LRRC49/CSTPP2, or PCM1 by IF using indicated antibodies. **c** RPE1 cells were infected with empty vector (EV), Flag-MAP4m, Flag-MAP4m–TTLL1 WT, or Flag-MAP4m–TTLL1 E326G lentiviruses for 72 h and immuno-stained or immuno-blotted with indicated antibodies. The intensity of endogenous MAP4 was quantified. $n \geq 60$ per sample were analyzed in three independent experiments. All data are presented as means ± SD. *$P < 0.05$ (unpaired *t*-test or Mann-Whitney test). Scale bars, 10 μm. A detailed description of quantification strategy is available in the Materials and Methods section.

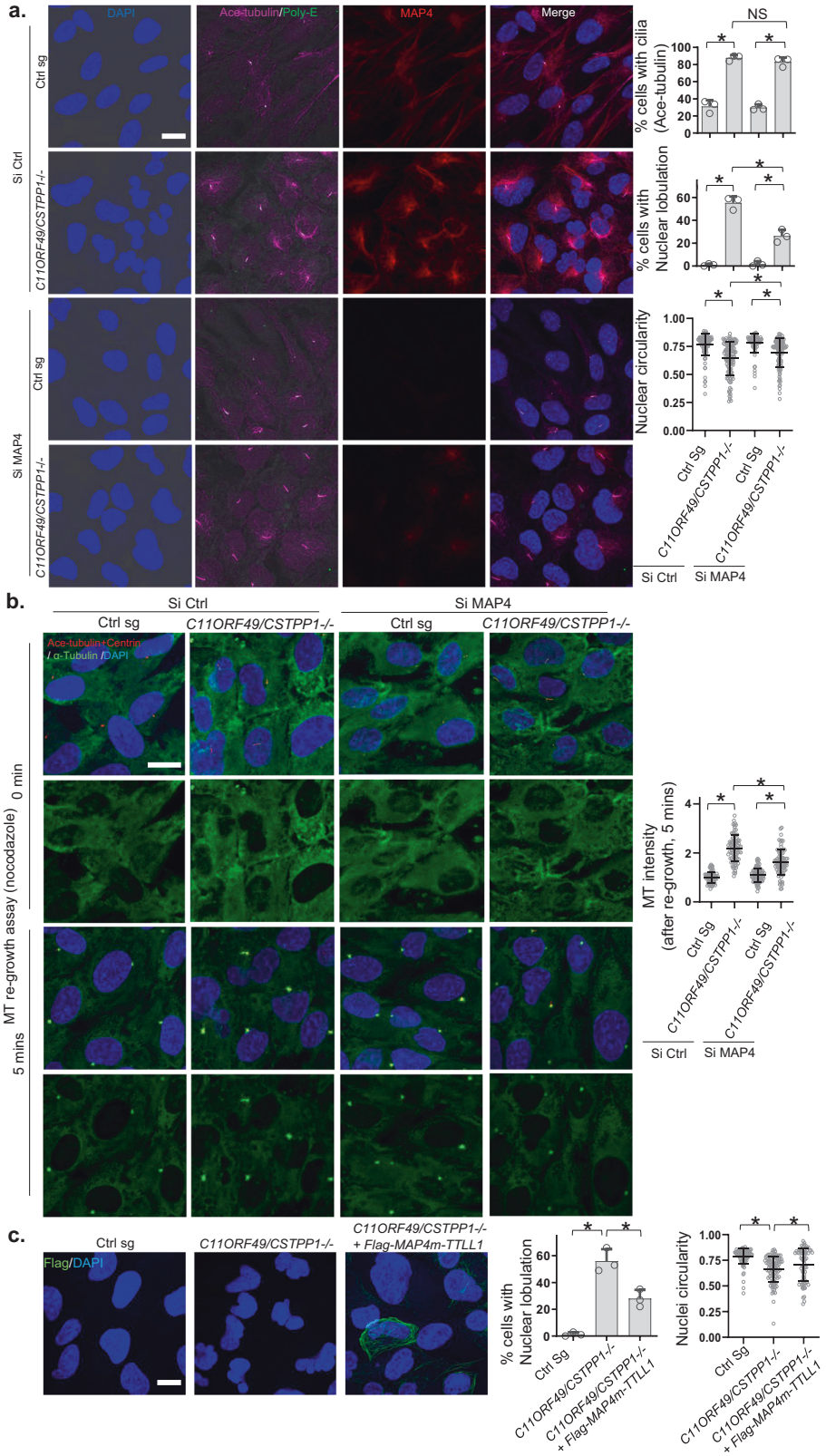

Fig. 7 Nuclear lobulation defects in *C11ORF49/CSTPP1*$^{-/-}$ cells result from aberrant MAP4 recruitment. a Cycling control and *C11ORF49/CSTPP1*$^{-/-}$ RPE1 cells were transfected with siRNAs against MAP4. Three days after transfection, cells were visualized with indicated antibodies to examine cilia and nuclear shape. **b** Control and *C11ORF49/CSTPP1*$^{-/-}$ RPE1 cells were transfected with siRNAs against MAP4 for 3 days. MT organization was examined after MT depolymerization (0 min, after 1 h treatment with nocodazole) and re-growth for 5 min after removal of drug by IF using α-tubulin antibody. Intensity of MT asters were quantified. **c** Nuclear shape was examined in control cells, *C11ORF49/CSTPP1*$^{-/-}$ cells, and *C11ORF49/CSTPP1*$^{-/-}$ cells infected with Flag-MAP4m–TTLL1 WT cells by IF using indicated antibodies. $n \geq 60$ per sample were analyzed in three independent experiments. Nuclei with > 2 lobes were defined as lobulated or multi-lobed. Circularity of nuclei was measured with CellProfiler software Form factor function. All data are presented as means ± SD. *$P < 0.05$ (unpaired *t*-test or Mann-Whitney test). Scale bars = 10 μm.

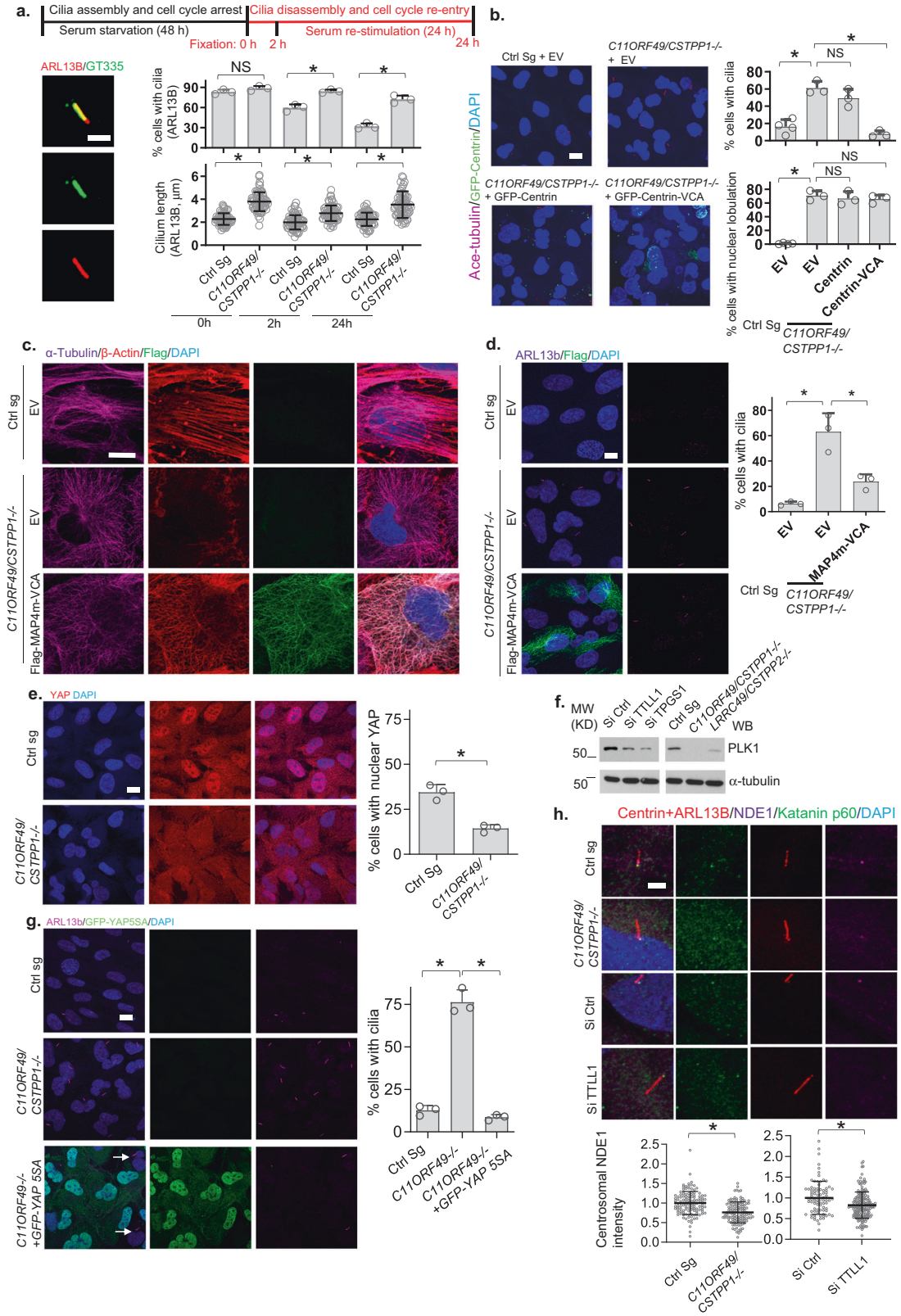

Loss of C11ORF49/CSTPP1 leads to ciliary defects and developmental abnormalities

The in vivo function of C11ORF49/CSTPP1 has not been studied in any animal model. Zebrafish C11ORF49/CSTPP1/zgc:92873 protein exhibits 56% similarity to its human homolog. Therefore, we investigated the function of C11ORF49/CSTPP1 in development by generating a *C11ORF49/CSTPP1*$^{-/-}$ zebrafish line using CRISPR/Cas9-based gene editing. After generating mutant alleles, which

Fig. 8 Enhanced ciliation in C11ORF49/CSTPP1- and TPGC- deficient cells results from defects in an actin-mediated cilium disassembly pathway. a Control and *C11ORF49/CSTPP1*$^{-/-}$ RPE-1 cells were serum-starved for 48 h and then re-stimulated with 10% FBS for the indicated times. Ciliation ratio and cilium length were measured and quantified at the indicated times. **b** Cycling control and *C11ORF49/CSTPP1*$^{-/-}$ RPE1 cells were infected with empty (EV), GFP-CENTRIN1, or GFP-CENTRIN1-VCA lentiviruses for 72 h and immuno-stained with indicated antibodies to examine ciliation and nuclear shape. **c**, **d**. Cycling control and *C11ORF49/CSTPP1*$^{-/-}$ RPE1 cells were infected with empty (EV), or Flag-MAP4m-VCA lentiviruses for 72 h and immuno-stained with indicated antibodies to examine ciliation and actin organization. **e** Cycling control and *C11ORF49/CSTPP1*$^{-/-}$ RPE1 cells were immuno-stained with indicated antibodies to examine YAP/TAZ localization. **f** Protein levels for PLK1 were examined in lysates from controls and cells depleted of indicated proteins by western blotting using indicated antibodies. **g** Cycling control and *C11ORF49/CSTPP1*$^{-/-}$ RPE1 cells were infected with or without GFP-YAP5SA for 72 h and immuno-stained with indicated antibodies to examine ciliation. Arrows indicate ciliated *C11ORF49/CSTPP1*$^{-/-}$ cells without expression of GFP-YAP5SA. **h** The intensity of centrosomal NDE1 was quantified in cycling, ciliated control RPE1 cells and cells depleted of TTLL1 or C11ORF49/CSTPP1 by IF using indicated antibodies. Scale bars, 2 μm in **a** and **h**. Scale bar, 10 μm in all other panels. $n \geq 60$ per sample were analyzed in three independent experiments in **a**, **f**. $n \geq 100$ per sample were analyzed in three independent experiments for all other data in this figure. All data are presented as means ± SD. *$P < 0.05$ (unpaired *t*-test or Mann-Whitney test).

are expected to lead to premature termination in the C11ORF49/CSTPP1 open reading frame, we in-crossed fish to produce homozygotes. Zebrafish C11ORF49/CSTPP1/zgc:92873 protein was undetectable in these mutants (Fig. 9a). We found that *C11ORF49/CSTPP1*$^{-/-}$ fish can survive to adulthood and produce offspring. Expression of zebrafish C11ORF49/CSTPP1 transcripts is elevated in ciliated tissues/organs, including brain, spinal cord, kidney, eyes, ears and lateral line[68] (Supplementary information, Fig. S9). We examined maternal zygotic (MZ) *C11ORF49/CSTPP1*$^{-/-}$ embryo development at 24 h post-fertilization (hpf) and 2 days post-fertilization (dpf) and found no morphological defects in a cohort of ciliated tissues, including the brain, eyes, ears, posterior lateral line primordium, and pronephros (Supplementary information, Fig. S10a). Next, we asked whether cilium disassembly in MZ *C11ORF49/CSTPP1*$^{-/-}$ zebrafish was dysregulated, as observed in human RPE1 KO cells. We found that the percentage of ciliated cells and ciliary length in Kupffer's Vesicle (KV), a transient, ciliated organ required to establish visceral laterality, were significantly increased, although such alterations were not observed in the ear, pronephros, or neural tube (Fig. 9b and Supplementary information, Fig. S10b–d). These data suggest that C11ORF49/CSTPP1 is involved in cilium disassembly in vivo and that its role is conserved in vertebrates. Since defective cilium disassembly of KV cilia has been reported to affect body patterning by perturbing left–right asymmetry,[65] we examined heart looping in MZ *C11ORF49/CSTPP1*$^{-/-}$ fish at 2 dpf. In zebrafish, the cardiac ventricular chamber bends rightward, beginning at 30 hpf, and the heart ultimately adopts an "S" shape at 48 hpf, a process referred to as cardiac looping. Strikingly, we observed a significant defect in heart looping, with an increased proportion of MZ *C11ORF49/CSTPP1*$^{-/-}$ embryos without a looped heart (Fig. 9c), suggesting that C11ORF49/CSTPP1-mediated cilium disassembly also plays an important role in maintaining laterality of the heart and body plan patterning. We examined actin organization in zebrafish KV and nuclear shape in muscle, eye, and heart, but detected no obvious defects (Supplementary information, Fig. S10e–h). These data suggest that, at least in KV, the regulation of cilium disassembly and nuclear lobulation by C11ORF49/CSTPP1 may be separable, and this observation comports with our ability to distinguish regulatory mechanisms in human RPE1 cells. Currently, however, we cannot rule out the possibility that there are nuclear shape or actin defects in other tissues or at different developmental stages. It is also possible that all functions of C11ORF49/CSTPP1 are not wholly conserved between zebrafish and humans, and in this respect, it is intriguing that zebrafish lack a *LRRC49/CSTPP2* homolog. We also cannot rule out the existence of a compensatory mechanism that prevents the formation of lobulated nuclei to facilitate organ development. Taken together with our in vitro data, we suggest that ablation of C11ORF49/CSTPP1 impairs cilium disassembly, which in turn leads to early KV and heart-looping defects in zebrafish.

DISCUSSION

In this study, we identified C11ORF49/CSTPP1 as a critical regulator of nuclear shape and cilium disassembly. We found that C11ORF49/CSTPP1 is a novel regulator of TPGC that controls the assembly and stability of this protein complex and modulates MT polyglutamylation and the recruitment of MAP4, which further regulates MT assembly and nuclear shape (Fig. 9d). We found that crippling TPGC activity leads to aberrant MAP4 recruitment and assembly of MTs that persist at the end of mitosis and penetrate the nucleus after NE re-assembly. We also showed that C11ORF49/CSTPP1 and TPGC modulate MT association of actin nucleators and MT–actin crosslinkers, and the disruption of this activity impairs an actin-dependent cilium disassembly pathway and leads to enhanced ciliogenesis and developmental disorders. Interestingly, although TPGC-associated proteins localize to CS and are trafficked along MT, the phenotypes associated with depletion of each subunit and PCM1 are not universal, suggesting subunit-specific roles.

Regulation of nuclear morphology and cilium disassembly by tubulin PTM

Our understanding of nuclear shape regulation largely derives from studies of structural proteins within the nucleus and nuclear envelope, and recent studies have focused on mechanisms that promote nuclear envelope assembly at the end of mitosis.[6] However, relatively little is known about how MT PTMs or dynamics or cytoplasmic proteins influence nuclear shape and nuclear reformation after mitosis. In this study, we identified a tubulin modifying enzyme complex TPGC, and its novel regulator, C11ORF49/CSTPP1, as essential regulators of nuclear shape. Specifically, we found that loss of C11ORF49/CSTPP1 or subunits within the TPGC can alter tubulin polyglutamylation levels and the binding of MAP4, which stimulates MT polymerization, resulting in formation of MTs that penetrate the nucleus and prevent proper nuclear reformation in late telophase, resulting in multi-lobulation. In addition, it is known that LINC components serve to bridge MT networks with the nuclear envelope, and our data suggest that abnormal increases in MAP4-mediated MT assembly could also create excessive mechanical forces and tension on the nuclear envelope, which in turn could contribute to nuclear lobulation. Recent studies also demonstrate the importance of removing MT through spastin cleavage to allow sealing of the nuclear envelope, thereby preventing the formation of multi-lobed nuclei,[50,51] and spastin-mediated severing is stimulated by polyglutamylation.[52,53] Notably, although we did not detect any differences in spastin localization in mitosis in our *C11ORF49/CSTPP1* KO cells (data not shown), we have shown that the MTs in *C11ORF49/CSTPP1* KO cells are less susceptible to spastin-mediated severing and can contribute to nuclear lobulation (Supplementary information, Fig. S7b). Interestingly, we did not observe nuclear lobulation after transient depletion of TPGS1 or TTLL1, despite observing decreased MT poly-E levels, increased MAP4 recruitment to MT,

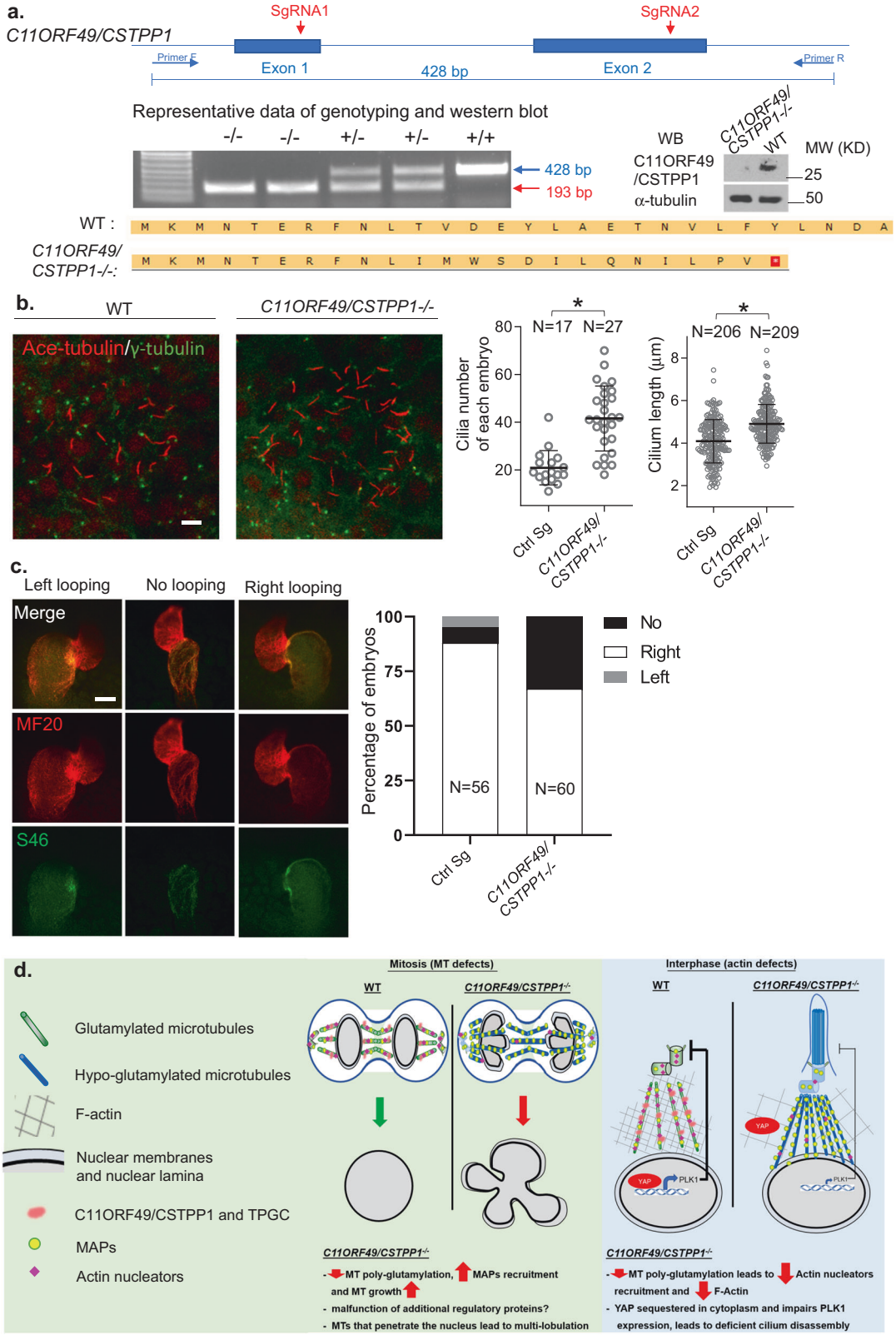

and increased MT assembly in these cells. These data indicate that the magnitude of MT-dependent mechanical forces generated by depletion of each subunit could vary, or there may be additional subunit-specific functions for C11ORF49/CSTPP1 and LRRC49/CSTPP2 that govern nuclear shape and that decreased MT polyglutamylation and increased MAP4 recruitment may not be sufficient to induce nuclear lobulation by themselves. We speculate that accessory factors could act in concert with C11ORF49/CSTPP1 and LRRC49/CSTPP2 to suppress nuclear lobulation.

Fig. 9 Loss of C11ORF49/CSTPP1 leads to developmental defects in zebrafish. a Strategy for making zebrafish C11ORF49/CSTPP1 KO strains by deletion of a genomic region between exons 1 and 2, resulting in an early stop mutation in exon 1 and the depletion of the protein, as indicated by western blotting assay (WB, right). **b** Whole-mount IF microscopy staining of cilia and centrosomes in the Kupffer's vesicle in embryos at the 6-somite stage using antibodies against acetylated α-tubulin and γ-tubulin. Ciliary length was measured based on acetylated α-tubulin and γ-tubulin staining. Scale bar, 5 μm. All data are presented as means ± SD. $*P < 0.05$ (unpaired *t*-test). **c** Ventral views of zebrafish hearts stained with MF20 (red) and S46 (green) antibodies to visualize the ventricle and atrium at 48 hpf. MF20 marks the entire heart and S46 marks the atrial myocardium. Scale bar, 50 μm. **d** Model for regulation of cytoskeleton dynamics, cilia disassembly, and nuclear shape by the C11ORF49/CSTPP1-TPGC. CS-localized C11ORF49/CSTPP1-TPGC maintains the level of MT polyglutamylation, which regulates the binding of MAPs and actin nucleators. Disruption of C11ORF49/CSTPP1-TPGC leads to elevated MT polymerization, and promotes nuclear lobulation by enhancing assembly of MTs that penetrate the nuclear envelope. On the other hand, C11ORF49/CSTPP1-TPGC regulates actin organization and expression/recruitment of cilium disassembly regulators, as the loss of these proteins leads to enhanced ciliogenesis, enhanced ciliary signaling, and developmental defects.

Before this study, the relationship between MT PTMs and actin organization had not been explored. Our data suggest that C11ORF49/CSTPP1-TPGC-mediated MT polyglutamylation is required to maintain normal actin as well as MT assembly, suggesting a major role for this complex in regulating the two major cytoskeletal networks. Mechanistically, we showed that recruitment of several actin nucleators and cross-linkers to MT was diminished in *C11ORF49/CSTPP1* KO and TTLL1-depleted cells (Fig. 3). Further, LINC proteins connect both actin and MT networks to the nuclear envelope,[6] and therefore lobulation could also result from disruption of the mechanical forces created by actin on the nuclear envelope. Although this possibility is currently under investigation, we found that restoration of the peri-centrosomal actin network rescued aberrant ciliation but did not alleviate nuclear shape defects in *C11ORF49/CSTPP1* KO cells. These findings, taken together with the observation that MT depolymerization or MAP4 depletion rescues lobulation, suggests that aberrations in nuclear shape may be most impacted by defects in MT networks.

Previous studies regarding the regulation of ciliogenesis by axoneme glutamylation yielded a complex picture, in part due to tissue- and species-specific roles for each tubulin glutamylation enzyme, with relatively few mechanistic insights. In this study, we found that C11ORF49/CSTPP1-TPGC-mediated tubulin polyglutamylation negatively regulates ciliogenesis in both human RPE1 cells and zebrafish. We demonstrated that aberrant ciliation in human cells likely stems from the ability of this complex to regulate binding of actin nucleators and MT–actin cross-linkers to MT, which in turn regulates an actin-dependent YAP-PLK1 cilium disassembly pathway. Thus, for the first time, our data demonstrate that MT polyglutamylation can regulate ciliogenesis by modulating an actin-dependent cilium disassembly pathway. Interestingly, we found that decreased levels of PLK1 in *C11ORF49/CSTPP1*$^{-/-}$ cells were associated with delays in cilium disassembly, although it did not compromise other PLK1-dependent roles in cell proliferation or mitosis. These data indicate that PLK1 protein levels required for cilium disassembly and mitosis could be different. Of note, a previous report indicated that short-term inhibition of PLK1 can kill tumor cells while sparing normal cells,[69] suggesting that normal cells can proliferate with decreased PLK1 levels.

The role of CSs as regulators of MT and actin dynamics has been explored in a limited way and has focused on their transport along MT to centrosomes.[30,31] Our data suggest that C11ORF49/CSTPP1 localizes to CS and directly binds to MT (Fig. 3), perhaps through multiple interaction surfaces, and thus, the protein may serve as a bridge between TPGC and MT. It is also possible that C11ORF49/CSTPP1 interacts with MT indirectly, through the other TPGC subunits, such as TPGS1, LRRC49/CSTPP2, and the catalytic subunit, TTLL1. The localization of TPGS1 and LRRC49/CSTPP1 to CS suggests that these two proteins may bind MT. Although a MT-binding domain conserved in other TTLL family members was not found in TTLL1,[49] it is still possible that TTLL1 uses an undisclosed domain to bind/recognize MT when forming a complex with C11ORF49/CSTPP1 and other TPGC subunits. Future structure-function experiments will be required to dissect the precise roles for each subunit in modulating MT binding. Nevertheless, for the first time, our data demonstrate that satellite-associated proteins also regulate MT polymerization by modulating tubulin PTM. Our study thus links CS-resident proteins and nuclear morphology for the first time. Our findings also expand our understanding of how CS modulate ciliogenesis, pinpointing PTM and actin organization as novel routes.

Thus far, little is known about how CSs regulate actin organization. A recent study suggests that CS proteins could regulate centrosomal actin organization by recruiting actin nucleators, such as WASH and ARP2, to centrosomes.[59] In this study, we propose a new model in which CS-associated proteins modulate MT polyglutamylation and thereby affect the recruitment of actin nucleators and actin–MT crosslinkers to MT. In this way, TPGC and associated proteins could regulate actin assembly, MT–actin crosslinking, and actin organization. Additional studies are needed to investigate how MT polyglutamylation regulates MT association of actin regulators, since we currently cannot exclude the possibility that C11ORF49/CSTPP1 and other TPGC subunits directly interact with and recruit actin nucleators. Moreover, we observe C11ORF49/CSTPP1- and LRRC49/CSTPP-2 positive granules in the cytoplasm that do not co-localize with PCM1 (Fig. 3c and Supplementary information, Fig. S4a), suggesting that these proteins could have CS-independent functions that contribute to cilium and nuclear shape defects observed herein. Despite these unanswered questions, it is clear that the proteins we have characterized in this study play a vital role in regulating cytoskeleton dynamics, nuclear shape, and cilium disassembly.

The function of C11ORF49/CSTPP1-TPGC axis in development and disease

The function of C11ORF49/CSTPP1 has not been studied in vivo in any animal model. Thus, we have also investigated the developmental impact of C11ORF49/CSTPP1 loss in zebrafish and found that cilium disassembly was defective in KV but not other tissues, suggesting that there may be genetic compensation, that C11ORF49/CSTPP1-TPGC functions in a tissue- or developmental stage-specific manner, or that distinct tissues are more or less affected when this complex is inactivated. We also found that cilium disassembly defects in the KV of *C11ORF49/CSTPP1*$^{-/-}$ fish lead to abnormal heart looping, which is consistent with other reports of left-right symmetry defects in cilium disassembly mutants after loss of NDE1.[65] Since C11ORF49/CSTPP1 and each of the TPGC subunits have common and unique binding partners and play different roles in regulating TPGC assembly and stability, knockouts for each gene may lead to overlapping but also distinct phenotypes in animal models. Indeed, while abnormal sperm morphology and function were observed in both *TPGS1* and *TTLL1* KO mice, chronic rhinosinusitis is only observed in *TTLL1* KO mice, and reduced body fat is only found in *TPGS1* KO mice.[12,15–17] These data and data from this study demonstrate extensive involvement of TPGC in various developmental processes.

A systematic characterization of mice lacking all TPGC subunits will be required to explain why PTMs must be strictly regulated by multiple TPGC subunits. We postulate that in addition to their role in the localization and stabilization of TPGC demonstrated herein, the subunits of this complex could play critical roles in enzyme activation and substrate targeting. There have been several reports showing that TTLLs modify substrates other than MT.[70–73] For example, it has been shown that histone chaperones and the transcription factor KLF4 are substrates of TTLL1 and TTLL4, and TTLL5 glutamylates the retinitis pigmentosa GTPase regulator (RPGR).[71–73] It is possible that TPGC subunits could also modulate TTLL1 activity toward other, yet-to-be-defined substrates and contribute to the regulation of cilium assembly, nuclear morphology, and other unexplored processes. Further, loss of these subunits could potentially explain some of the phenotypes observed in our study if substrate specificity or targeting of the complex were compromised in depleted cells.

MATERIALS AND METHODS

Cell culture and gene-editing using CRISPR/Cas9

Human retinal pigment epithelial (RPE1-hTERT) and human embryonic kidney (HEK293T) cells were obtained from ATCC. Cells were grown in DMEM supplemented with 10% FBS. RPE1 cells were incubated in DMEM without FBS for 48 h to induce cilia formation and then incubated in DMEM with FBS to induce cilia disassembly. To generate CRISPR KO cells, RPE1 cells were infected with lentivirus expressing Flag-Cas9 and sgRNA and grown for 10 days, after which the cells were examined by IF and separated as single cells into 96-well plates. After 2 weeks, the colonies were analyzed for genome editing. C11ORF49/CSTPP1 Flag Knock in RPE1 cells were made by incorporating mAID-Flag tag into the native C11ORF49/CSTPP1 locus. sgRNAs used included: sg CTL (5′-GAGACGTCTAGCACGTCTCT-3′), sg *C11ORF49/CSTPP1* (5-CAAACAGTGATATTCTTTCA-3′), and sg *LRRC49/CSTPP2* (5-TCAGAAGAACGTTGAAGAAT-3′).

Bio-ID proximity labeling

Stable RPE1 cell lines expressing Flag-BirA, Flag-BirA-TALPID3, and Flag-BirA-C2CD3 were cultured in medium containing 50 mM biotin for 24 h. Twenty 15-cm dishes for each cell line were washed with PBS and lysed in 10 mL lysis buffer (50 mM Tris-HCl, pH 7.5, 150 mM NaCl, 1 mM EDTA, 1 mM EGTA, 1% Triton X-100, 0.1% SDS, 1:500 protease inhibitor cocktail (Sigma-Aldrich), 1:1000 benzonase nuclease (Novagen) and incubated at 4 °C for 1 h, briefly sonicated to disrupt any visible aggregates, then centrifuged at 16,000× *g* for 30 m at 4 °C. Supernatant was incubated with Streptavidin-sepharose (GE) for 3 h at 4 °C with end-over-end rotation. Beads were washed with lysis buffer and 3 times with 50 mM ammonium bicarbonate (pH 8.3). Mass spectrometric (MS) analysis was performed after tryptic digestion with MS-grade TPCK trypsin (Promega, Madison, WI), and then half of the supernatant was analyzed per MS run.

Transfection and lentivirus infection

Polyethylenimine was used for plasmid transfections in 293T cells. DNA and PEI (1 mg/mL) were added at 1:5 to 1:8 ratio. Lentiviral supernatant was prepared by co-transfection of the lentiviral plasmid with Δ8.2 envelope and VsVG packaging plasmids into 293T cells using PEI. Lentivirus supernatants were harvested 48 h–72 h post-transfection. RPE1 cells were incubated with viral supernatants and 8 μg/mL polybrene for 6 h–10 h, and medium was changed thereafter. siRNAs were transfected into RPE1 cells using RNAiMAX (Invitrogen, Carlsbad, CA) according to the manufacturer's protocol. siRNAs were synthesized by Dharmacon with the following sequences: non-specific control (5′-AATTCTCCGAACGTGTCACGT-3′), PCM1 (5′-GGCUUUAACUAAUUAU GGAdTdT-3′), MAP4 (5′-GAUGAGAACGGGUGUGUAU-3′), siRNA pool against TPGS1 (M-023892-01-0005), siRNA pool against TTLL1 (M-009556-01-0005), siRNA pool against LRRC49/CSTPP2 (M-020660-01-0005), and siRNA pool against MAP4 (M-011724-01-0005).

DNA constructs

To generate Flag-tagged proteins, human C11ORF49/CSTPP1, LRRC49/CSTPP2, TPGS1, TPGS2, TTLL1, and NICN1 cDNA were obtained from Sino Biological US Inc (Wayne, PA, USA) and cloned into PCDH-CMV-Flag-Neo vector. To generate the PCDH-CMV-FLAG-MAP4m plasmid, MAP4m was amplified by PCR from MSCV–CMV–CFP–FRB–MAP4m[26] and subcloned into PCDH-CMV-FLAG. To generate PCDH-CMV-TTLL1-FLAG-MAP4m plasmid, MAP4m was amplified by PCR from MSCV–CMV–CFP–FRB–MAP4m plasmid[26] and subcloned into PCDH-CMV-TTLL1-Flag. PCDH-CMV-TTLL1-FLAG-MAP4m-E326G mutant was generated by site-directed mutagenesis. To generate pCDH-CMV-EGFP-CENTRIN1-VCA, EGFP-CENTRIN1-VCA was sub-cloned from pEGFP-C1-Centrin1-VCA[61] into PCDH-CMV-Flag-Neo vector. To generate the PCDH-CMV-FLAG-MAP4m-VCA plasmid, VCA was amplified by PCR from pCDH-CMV-EGFP-CENTRIN1-VCA and subcloned into PCDH-CMV-FLAG-MAP4m. pLenti-EB1-EGFP was a gift from Ken-Ichi Takemaru (Addgene # 118084). All PCR reactions were performed using high fidelity Herculase II Fusion DNA Polymerase (Agilent), and the PCR-generated plasmids were further verified by DNA sequencing. Drs. D.-S. Lim and J. Kim (KAIST, South Korea) provided YAP-5SA.

Immunoprecipitations

293T cells were lysed in ELB buffer (50 mM Hepes, pH 7, 150 mM NaCl, 5 mM EDTA, pH 8, 0.1% NP-40, 1 mM DTT, 0.5 mM AEBSF, 2 μg/mL leupeptin, 2 μg/mL aprotinin, 10 mM NaF, 50 mM β-glycerophosphate, and 10% glycerol) on ice, lysates were centrifuged, and supernatants were incubated with 2 μg antibody and Protein A/G Sepharose (GE17-0780-01 and 17-0618-01, GE Healthcare) or Flag beads (A2220, Sigma-Aldrich). For immunoprecipitation, 2 mg of the resulting supernatant was immunoprecipitated, and beads were washed with ELB buffer and analyzed by immunoblotting.

Preparation of total cytosolic fractions and polymerized MT fractions

Total cytosolic fractions and polymerized MT fractions were prepared as described earlier with minor modifications.[20] Cells were washed twice with PEM (80 mM PIPES, 2 mM EGTA, 1 mM $MgCl_2$, pH 6.9) at 37 °C, and permeabilized using PEM supplemented with 0.05% Triton X-100 and a protease inhibitors cocktail (Sigma) for 3 min at 37 °C, to collect all the cytosol proteins and unpolymerized tubulin (hereafter termed the Cyto-fraction). After a rapid wash with PEM, MTs were depolymerized in ice-cold PM (80 mM PIPES, 1 mM $MgCl_2$, pH 6.9) containing 5 mM CaCl2 and supplemented with protease inhibitors cocktail (MilliporeSigma) at 4 °C for 1 h. The MT-associated proteins and the formerly polymerized tubulin subunits that were collected at this stage were termed the MT-fraction. The Cyto and MT fractions were concentrated in Amicon Ultra filters (MilliporeSigma) and subjected to western blot analysis.

MT-binding protein spin-down assay

MT binding assays were performed with the Microtubule Binding Protein Spin-Down Assay Biochem Kit (Cytoskeleton, Inc.), according to the manufacturer's instructions. Flag-C11ORF49/CSTPP1 was expressed in HEK293T cells, transfected cells were lysed, and extracts were incubated with anti-Flag (M2) agarose beads (Sigma) for 2 h at 4 °C. Beads were washed with ELB buffer containing 500 mM NaCl. Purified proteins were eluted with 1 mg/mL Flag peptide in elution buffer (100 mM Tris, pH8, 50 mM NaCl, 1 mM $MgCl_2$, 1 mM DTT and 0.1% Triton X-100) and dialyzed against PIPES buffer (80 mM piperazine-N, N′-bis (2-ethanesulfonic acid) (PIPES) pH 6.9, 1 mM ethylene glycol tetraacetic acid, 1 mM $MgCl_2$, 50 mM NaCl, and 1 mM DTT) prior to usage in binding assays.

MT tracking

Live-cell images of GFP-EB1 were recorded at 1.5-s intervals for 60 frames, using a 63× oil objective. MTs were automatically tracked in a centrosomes-centered square (length = 10 μm) using PlusTipTracker software as described previously.[74] The same set of parameters was used for all movies: 5 minimum and 8 maximum frames for gap length; 25° and 10° for maximum forward and backward angles; 3–24 pixels as a search radius,10 pixels for fluctuation radius; and 74 nm for pixel size.

IF microscopy

Cells were fixed with cold methanol or with 10% formalin solution (Sigma-Aldrich) and permeabilized with 0.3% Triton X-100/PBS. For MT Poly-E staining, cells were fixed with 0.5% Glutaraldehyde in PEM buffer (80 mM PIPES, 5 mM EGTA, 1 mM $MgCl_2$, 0.3% Triton X-100) for 10 min followed by three PBS washes and quenching with 0.1% $NaBH_4$ in PBS for 10 min. Slides were blocked with 3% BSA in PBS before incubation with primary antibodies. Secondary antibodies used were Alexa Fluor 488-conjugated,

Alexa Fluor 568-conjugated or Alexa Fluor 647-conjugated (Invitrogen) donkey anti-mouse, anti-rabbit, or anti-goat IgG. Cells were stained with DAPI, and slides were mounted, observed, and photographed using an LSM 800 confocal microscope (63×, NA 1.4 Carl Zeiss) with Zen software (Carl Zeiss). Image analysis was performed using Photoshop (Adobe). The intensity of α-tubulin, Poly-E, MAP4, and NDE1 was quantified by Image J. Briefly, regions of interest were defined by drawing a circle (radius of 4.35 μm for Poly-E and MAP4, 1.8 μm for α-tubulin, and 0.8 μm for NDE1) centered on the centrosome. Background values measured from the same-sized circle in an adjacent region were subtracted, and the resulting intensity was normalized to the averaged intensity of the control sample in each experiment. For the analysis of MT organization and ciliation during mitosis, RPE1 cells were treated with a double-thymidine block and released to enrich for mitotic cells. Cells with two centrin 2 dots were counted as G1-phase cells; those with three to four clustered centrin 2 dots as S-phase cells; and those with three to four centrin-2 dots, in which two pairs of dots were at least 3 μm apart, were counted as G2-phase cells. Mitotic stages were identified by chromosome distribution and spindle formation. Confocal *z*-stacks were scanned through the entire nucleus at 0.45-μm intervals. MTs were scored as penetrating the nucleus when confocal *z*-slices above and below had nuclear staining but no MTs, and thus the observed MTs had been trapped within the nucleus. High-resolution IF imaging of MTs was carried out using a Zeiss Confocal 800 Airyscan system. Circularity of nuclei was measured with CellProfiler software's form factor function.

Correlative light and electron microscopy (CLEM)

CLEM was performed at the NYU School of Medicine Microscopy Laboratory. Briefly, cells were plated on gridded glass-bottom dishes (P35G-1.5-14-CGRD, MatTek) and fixed with 2% paraformaldehyde and 0.1% glutaraldehyde in 0.1 M sodium phosphate buffer for 15 min at room temperature. Cells were permeabilized with 0.06% Triton X-100 in PBS for 10 min, followed by incubating in blocking solution consisting of 5% bovine serum albumin, 0.4% goat serum, and 0.1% cold water fish gelatin in PBS for 60 min at room temperature. Antibody labeling was performed by incubating the cells with antibodies against anti-α-tubulin (T5168a, Sigma) in antibody incubation buffer consisting of 1% BSA and 0.1% cold water fish gelatin in PBS at 4 °C overnight. FluoroNanogold (Goat anti-mouse Alexa Fluor® 546, Nanoprobes 7402) in PBS-Milk buffer (1% Non-fat dried milk, 0.05 Tween 20, 20 mM Phosphate and 150 mM NaCl, pH 7.4) was added to the cells and incubated at 4 °C overnight. After each antibody incubation, cells were washed in PBS-Milk buffer for 10 min at room temperature on a shaker. Cells were then incubated with DAPI in PBS and washed with PBS several times at room temperature. Fluorescent signal was visualized using a Zeiss Axio Observer microscope, and high and low magnification images were taken at regions of interest. Silver enhancement was performed with HQ Silver enhancement kit (Nanoprobes). Then cells were fixed with 2.5% glutaraldehyde for 30 min, post fixed with 0.5% osmium tetroxide for 10 min, in block stained with 1% uranyl acetate for 1 h, then dehydrated in ethanol, and embedded in Araldilte 502 (Electron Microscopy Sciences). The sample blocks were removed by immersing the whole dish in liquid nitrogen, and trimmed under stereoscope. The grid pattern imprinted in the resin served as the landmark to correlate light microscopy images. Serial thin (100 nm) sections were cut using Leica UC6 ultramicrotome, collected on formvar-coated slotted copper grids, and stained with uranyl acetate and lead citrate. Stained grids were examined using an electron microscope (FEI Talos 120 C) and photographed with a Gatan OneView 4-k × 4-k camera (Gatan, Inc.).

MT re-growth assays

To perform MT re-growth assays, cells grown on cover glasses were treated with 10 μM nocodazole in DMEM at 37 °C or placed in ice water for 1 h to depolymerize MT. MT re-growth was initiated at 37 °C and allowed to proceed for various time periods. Cells were fixed at room temperature with 4% paraformaldehyde in PEM buffer (80 mM PIPES, pH 6.9, 1 mM $MgCl_2$, 5 mM EGTA, 0.5% Triton X-100) and permeabilized with 0.3% PBST (PBS with Triton X-100), followed by a conventional IF protocol.

Antibodies

Antibodies used in our study include: mouse anti-centrin (1:2500 for IF, 04-1624; Millipore), rabbit anti-Flag (1:2000 for WB, F7425, Sigma), mouse anti-Flag (1:2000 for WB and 1:500 for IF, F1804, Sigma), goat anti-GFP (1:500 for IF, ab545025, Abcam), mouse anti-α-tubulin (1:500 for IF and 1:5000 for WB, T5168, Sigma), mouse anti-Acetyl-α-Tubulin (1:2000 for IF, T7451, Sigma), goat anti-γ-tubulin (1:500 for IF, sc-7396, Santa Cruz), mouse anti-glutamylated tubulin (GT335) (1:2500 for IF, AG-20B-0020-C100, Adipogen), rabbit anti-PolyE (1:1000 for IF and 1:200 for WB, A26381411, Adipogen), rabbit anti-Arl13b (1:2000 for IF, 17711-1-AP, Proteintech), Alexa fluor 488 phalloidin (1:50 for IF, A12379, Invitrogen), rabbit anti-C11ORF49 (1:1000 for WB, HPA040051, Sigma), rabbit anti-LRRC49 (1:1000 for WB, ab189250, Abcam), rabbit anti-TPGS1 (1:1000 for WB, ab184178, Abcam), rabbit anti-TPGS2[13] (1:4000 for WB), rabbit anti-TTLL1[13] (1:4000 for WB), rabbit anti-TTLL1, (2 μg for IP of 2 mg cell lysis, Invitrogen PA5-27285), pig anti-TTLL1[17] (1:2000 for WB), rabbit anti-PCM1 (1:2000 for WB and 1:500 for IF, sc-67204, Santa Cruz), mouse anti-MAP4 (1:100 for IF, sc-390286, Santa Cruz), rabbit anti-MAP1S (1:1000 for WB, 15695-1-AP, Proteintech), mouse anti-SEPTIN2 (1:1000 for WB, 60075-1-Ig, Proteintech), rabbit anti-N-WASP (1:1000 for WB, 4848 T, Cell Signaling), rabbit anti-PROFILIN1 (1:1000 for WB, P7749, MilliporeSigma), rabbit anti-ARP2 (1:1000 for WB, ab47654, Abcam), mouse anti-NDE1 (1:100 for IF, sc-100328, Santa Cruz), mouse anti-MHC (1:20 for IF, MF20, DSHB), mouse anti-sd-MyHC (1:20 for IF, S46, DSHB), mouse anti-PLK1 (1:500 for IF, BD biosciences 558400), rabbit anti-HDAC6 (1:200 for IF, 07-732, MilliporeSigma), rabbit anti-Kif24 (1:200 for IF), mouse anti-Nek2 (1:100 for IF, 610593, BD Biosciences), rabbit anti-phosphorylated Tctex-1 (1:100 for IF), rabbit anti-Phospho-Aurora A (Thr288) (1:2000 for IF, 2914, Cell Signaling), rabbit anti-KIF2A (1:200 for IF, PAB12407, Abnova), rabbit anti-KATNA1 (1:100 for IF, 17560-1-AP, Proteintech).

Zebrafish husbandry and IF

Zebrafish care and use of live fish for experiments were approved and overseen by the New York University School of Medicine Institutional Animal Care and Use Committee. Embryos were raised at 28 °C in fish water. The following sgRNAs were co-injected together with Cas9 protein into Tg(cldnB:lyn2-GFP) embryos to generate the *C11ORF49/CSTPP1* mutant fish, sg*C11ORF49/CSTPP1* Zebrafish 1 (5′-CTAAATATTCGTCAA CGGTG-3′), and sg*C11ORF49/CSTPP1* Zebrafish 2 (5′-GGAATACACACAAT TTGGTG-3′). The resulting *C11ORF49/CSTPP1* mutant allele contains a 97-nt deletion and 3-nt insertion between exon 1 and 2, which results in a premature stop codon. For immunostaining, embryos were fixed in 4% PFA at 4 °C overnight and permeabilized in methanol at −20 °C, rehydrated, and permeabilized with 10 μg/mL proteinase K in 1× PBS. 0.1% Tween-20 (PBST) at room temperature. Embryos were then blocked in 3% BSA in PBST for 1 h and incubated in primary antibody at 4 °C overnight. Following PBST washes, they were incubated in secondary antibody overnight at 4 °C.

Statistics and reproducibility

The statistical significance of the difference between two means was determined using a two-tailed unpaired Student's *t*-test or Mann-Whitney test of Prism Graphpad software. All data are presented as means ± SD as specified in figure legends. Differences were considered significant when $P < 0.05$. Results reported are from 3 independent biological replicates as noted in legends with reproducible findings each time. For all experiments, except as noted, $n \geq 100$ cells per sample were counted in three biologically independent experiments.

REFERENCES

1. Davidson, P. M. & Lammerding, J. Broken nuclei-lamins, nuclear mechanics, and disease. *Trends Cell Biol.* **24**, 247–256 (2014).
2. Skinner, B. M. & Johnson, E. E. Nuclear morphologies: their diversity and functional relevance. *Chromosoma* **126**, 195–212 (2017).
3. Manley, H. R., Keightley, M. C. & Lieschke, G. J. The neutrophil nucleus: an important influence on neutrophil migration and function. *Front. Immunol.* **9**, 2867 (2018).
4. Burke, B. & Stewart, C. L. The laminopathies: the functional architecture of the nucleus and its contribution to disease. *Annu. Rev. Genomics Hum. Genet.* **7**, 369–405 (2006).
5. Chow, K. H., Factor, R. E. & Ullman, K. S. The nuclear envelope environment and its cancer connections. *Nat. Rev. Cancer* **12**, 196–209 (2012).
6. Lele, T. P., Dickinson, R. B. & Gundersen, G. G. Mechanical principles of nuclear shaping and positioning. *J. Cell Biol.* **217**, 3330–3342 (2018).
7. Larrieu, D., Britton, S., Demir, M., Rodriguez, R. & Jackson, S. P. Chemical inhibition of NAT10 corrects defects of laminopathic cells. *Science* **344**, 527–532 (2014).
8. Olins, A. L. & Olins, D. E. Cytoskeletal influences on nuclear shape in granulocytic HL-60 cells. *BMC Cell Biol.* **5**, 30 (2004).

9. Janke, C. & Magiera, M. M. The tubulin code and its role in controlling microtubule properties and functions. *Nat. Rev. Mol. Cell Biol.* **21**, 307–326 (2020).
10. Bodakuntla, S., Jijumon, A. S., Villablanca, C., Gonzalez-Billault, C. & Janke, C. Microtubule-associated proteins: structuring the cytoskeleton. *Trends Cell Biol.* **29**, 804–819 (2019).
11. Magiera, M. M., Singh, P., Gadadhar, S. & Janke, C. Tubulin posttranslational modifications and emerging links to human disease. *Cell* **173**, 1323–1327 (2018).
12. Janke, C. et al. Tubulin polyglutamylase enzymes are members of the TTL domain protein family. *Science* **308**, 1758–1762 (2005).
13. Regnard, C. et al. Characterisation of PGs1, a subunit of a protein complex co-purifying with tubulin polyglutamylase. *J. Cell Sci.* **116**, 4181–4190 (2003).
14. van Dijk, J. et al. A targeted multienzyme mechanism for selective microtubule polyglutamylation. *Mol. Cell* **26**, 437–448 (2007).
15. Ikegami, K. et al. Loss of alpha-tubulin polyglutamylation in ROSA22 mice is associated with abnormal targeting of KIF1A and modulated synaptic function. *Proc. Natl. Acad. Sci. USA* **104**, 3213–3218 (2007).
16. Campbell, P. K. et al. Mutation of a novel gene results in abnormal development of spermatid flagella, loss of intermale aggression and reduced body fat in mice. *Genetics* **162**, 307–320 (2002).
17. Ikegami, K., Sato, S., Nakamura, K., Ostrowski, L. E. & Setou, M. Tubulin polyglutamylation is essential for airway ciliary function through the regulation of beating asymmetry. *Proc. Natl. Acad. Sci. USA* **107**, 10490–10495 (2010).
18. Vogel, P., Hansen, G., Fontenot, G. & Read, R. Tubulin tyrosine ligase-like 1 deficiency results in chronic rhinosinusitis and abnormal development of spermatid flagella in mice. *Vet. Pathol.* **47**, 703–712 (2010).
19. Spiliotis, E. T. Spatial effects - site-specific regulation of actin and microtubule organization by septin GTPases. *J. Cell Sci.* **131**, jcs207555 (2018).
20. Targa, B. et al. Septin filament coalignment with microtubules depends on SEPT9_i1 and tubulin polyglutamylation, and is an early feature of acquired cell resistance to paclitaxel. *Cell Death Dis.* **10**, 54 (2019).
21. Fernandez-Barrera, J. & Alonso, M. A. Coordination of microtubule acetylation and the actin cytoskeleton by formins. *Cell Mol. Life Sci.* **75**, 3181–3191 (2018).
22. Pinto-Costa, R. & Sousa, M. M. Profilin as a dual regulator of actin and microtubule dynamics. *Cytoskeleton* **77**, 76–83 (2020).
23. Wang, L. & Dynlacht, B. D. The regulation of cilium assembly and disassembly in development and disease. *Development* **145**, 1–13 (2018).
24. Anvarian, Z., Mykytyn, K., Mukhopadhyay, S., Pedersen, L. B. & Christensen, S. T. Cellular signalling by primary cilia in development, organ function and disease. *Nat. Rev. Nephrol.* **15**, 199–219 (2019).
25. Nachury, M. V. & Mick, D. U. Establishing and regulating the composition of cilia for signal transduction. *Nat. Rev. Mol. Cell Biol.* **20**, 389–405 (2019).
26. Hong, S. R. et al. Spatiotemporal manipulation of ciliary glutamylation reveals its roles in intraciliary trafficking and Hedgehog signaling. *Nat. Commun.* **9**, 1732 (2018).
27. O'Hagan, R. et al. Glutamylation regulates transport, specializes function, and sculpts the structure of cilia. *Curr. Biol.* **27**, 3430–3441.e3436 (2017).
28. Wloga, D., Joachimiak, E., Louka, P. & Gaertig, J. Posttranslational modifications of tubulin and cilia. *Cold Spring Harb. Perspect. Biol.* **9**, a028159 (2017).
29. Kubo, T., Hirono, M., Aikawa, T., Kamiya, R. & Witman, G. B. Reduced tubulin polyglutamylation suppresses flagellar shortness in Chlamydomonas. *Mol. Biol. Cell* **26**, 2810–2822 (2015).
30. Hori, A. & Toda, T. Regulation of centriolar satellite integrity and its physiology. *Cell Mol. Life Sci.* **74**, 213–229 (2017).
31. Prosser, S. L. & Pelletier, L. Centriolar satellite biogenesis and function in vertebrate cells. *J. Cell Sci.* **133**, jcs239566 (2020).
32. Dammermann, A. & Merdes, A. Assembly of centrosomal proteins and microtubule organization depends on PCM-1. *J. Cell Biol.* **159**, 255–266 (2002).
33. Hori, A., Ikebe, C., Tada, M. & Toda, T. Msd1/SSX2IP-dependent microtubule anchorage ensures spindle orientation and primary cilia formation. *EMBO Rep.* **15**, 175–184 (2014).
34. Kim, K. & Rhee, K. The pericentriolar satellite protein CEP90 is crucial for integrity of the mitotic spindle pole. *J. Cell Sci.* **124**, 338–347 (2011).
35. Kodani, A., Tonthat, V., Wu, B. & Sutterlin, C. Par6 alpha interacts with the dynactin subunit p150 Glued and is a critical regulator of centrosomal protein recruitment. *Mol. Biol. Cell* **21**, 3376–3385 (2010).
36. Sedjai, F. et al. Control of ciliogenesis by FOR20, a novel centrosome and pericentriolar satellite protein. *J. Cell Sci.* **123**, 2391–2401 (2010).
37. Gheiratmand, L. et al. Spatial and proteomic profiling reveals centrosome-independent features of centriolar satellites. *EMBO J.* **38**, e101109 (2019).
38. Gupta, G. D. et al. A dynamic protein interaction landscape of the human centrosome-cilium interface. *Cell* **163**, 1484–1499 (2015).
39. Wang, L., Failler, M., Fu, W. & Dynlacht, B. D. A distal centriolar protein network controls organelle maturation and asymmetry. *Nat. Commun.* **9**, 3938 (2018).
40. Gingras, A. C., Abe, K. T. & Raught, B. Getting to know the neighborhood: using proximity-dependent biotinylation to characterize protein complexes and map organelles. *Curr. Opin. Chem. Biol.* **48**, 44–54 (2019).
41. Luke, Y. et al. Nesprin-2 Giant (NUANCE) maintains nuclear envelope architecture and composition in skin. *J. Cell Sci.* **121**, 1887–1898 (2008).
42. Nachury, M. V. et al. A core complex of BBS proteins cooperates with the GTPase Rab8 to promote ciliary membrane biogenesis. *Cell* **129**, 1201–1213 (2007).
43. Wang, L., Lee, K., Malonis, R., Sanchez, I. & Dynlacht, B. D. Tethering of an E3 ligase by PCM1 regulates the abundance of centrosomal KIAA0586/Talpid3 and promotes ciliogenesis. *Elife* **5**, e12950 (2016).
44. Mikule, K. et al. Loss of centrosome integrity induces p38-p53-p21-dependent G1-S arrest. *Nat. Cell Biol.* **9**, 160–170 (2007).
45. Nguyen, H. L. et al. Overexpression of full- or partial-length MAP4 stabilizes microtubules and alters cell growth. *J. Cell Sci.* **110**, 281–294 (1997).
46. Nguyen, H. L., Gruber, D. & Bulinski, J. C. Microtubule-associated protein 4 (MAP4) regulates assembly, protomer-polymer partitioning and synthesis of tubulin in cultured cells. *J. Cell Sci.* **112**, 1813–1824 (1999).
47. Ghossoub, R. et al. Septins 2, 7 and 9 and MAP4 colocalize along the axoneme in the primary cilium and control ciliary length. *J. Cell Sci.* **126**, 2583–2594 (2013).
48. Zahnleiter, D. et al. MAP4-dependent regulation of microtubule formation affects centrosome, cilia, and Golgi architecture as a central mechanism in growth regulation. *Hum. Mutat.* **36**, 87–97 (2015).
49. Garnham, C. P. et al. Multivalent microtubule recognition by tubulin tyrosine ligase-like family glutamylases. *Cell* **161**, 1112–1123 (2015).
50. Ventimiglia, L. N. et al. CC2D1B coordinates ESCRT-III activity during the mitotic reformation of the nuclear envelope. *Dev. Cell* **47**, 547–563.e546 (2018).
51. Vietri, M. et al. Spastin and ESCRT-III coordinate mitotic spindle disassembly and nuclear envelope sealing. *Nature* **522**, 231–235 (2015).
52. Lacroix, B. et al. Tubulin polyglutamylation stimulates spastin-mediated microtubule severing. *J. Cell Biol.* **189**, 945–954 (2010).
53. Sandate, C. R., Szyk, A., Zehr, E. A., Lander, G. C. & Roll-Mecak, A. An allosteric network in spastin couples multiple activities required for microtubule severing. *Nat. Struct. Mol. Biol.* **26**, 671–678 (2019).
54. Pugacheva, E. N., Jablonski, S. A., Hartman, T. R., Henske, E. P. & Golemis, E. A. HEF1-dependent Aurora A activation induces disassembly of the primary cilium. *Cell* **129**, 1351–1363 (2007).
55. Cao, J. et al. miR-129-3p controls cilia assembly by regulating CP110 and actin dynamics. *Nat. Cell Biol.* **14**, 697–706 (2012).
56. Kim, S., Lee, K., Choi, J. H., Ringstad, N. & Dynlacht, B. D. Nek2 activation of Kif24 ensures cilium disassembly during the cell cycle. *Nat. Commun.* **6**, 8087 (2015).
57. Saito, M. et al. Tctex-1 controls ciliary resorption by regulating branched actin polymerization and endocytosis. *EMBO Rep.* **18**, 1460–1472 (2017).
58. Yeyati, P. L. et al. KDM3A coordinates actin dynamics with intraflagellar transport to regulate cilia stability. *J. Cell Biol.* **216**, 999–1013 (2017).
59. Farina, F. et al. The centrosome is an actin-organizing centre. *Nat. Cell Biol.* **18**, 65–75 (2016).
60. Rottner, K., Faix, J., Bogdan, S., Linder, S. & Kerkhoff, E. Actin assembly mechanisms at a glance. *J. Cell Sci.* **130**, 3427–3435 (2017).
61. Obino, D. et al. Actin nucleation at the centrosome controls lymphocyte polarity. *Nat. Commun.* **7**, 10969 (2016).
62. Kim, J. et al. Actin remodelling factors control ciliogenesis by regulating YAP/TAZ activity and vesicle trafficking. *Nat. Commun.* **6**, 6781 (2015).
63. Zhao, B. et al. Inactivation of YAP oncoprotein by the Hippo pathway is involved in cell contact inhibition and tissue growth control. *Genes Dev.* **21**, 2747–2761 (2007).
64. Gabriel, E. et al. CPAP promotes timely cilium disassembly to maintain neural progenitor pool. *EMBO J.* **35**, 803–819 (2016).
65. Kim, S. et al. Nde1-mediated inhibition of ciliogenesis affects cell cycle re-entry. *Nat. Cell Biol.* **13**, 351–360 (2011).
66. Lee, K. H. et al. Identification of a novel Wnt5a-CK1varepsilon-Dvl2-Plk1-mediated primary cilia disassembly pathway. *EMBO J.* **31**, 3104–3117 (2012).
67. Miyamoto, T. et al. The microtubule-depolymerizing activity of a mitotic kinesin protein KIF2A drives primary cilia disassembly coupled with cell proliferation. *Cell Rep.* **10**, 664–673 (2015).
68. Farnsworth, D. R., Saunders, L. M. & Miller, A. C. A single-cell transcriptome atlas for zebrafish development. *Dev. Biol.* **459**, 100–108 (2020).
69. Guan, R. et al. Small interfering RNA-mediated Polo-like kinase 1 depletion preferentially reduces the survival of p53-defective, oncogenic transformed cells and inhibits tumor growth in animals. *Cancer Res.* **65**, 2698–2704 (2005).
70. Xiong, Z. et al. Glutamylation of deubiquitinase BAP1 controls self-renewal of hematopoietic stem cells and hematopoiesis. *J. Exp. Med.* **217**, e20190974 (2020).
71. Ye, B. et al. Klf4 glutamylation is required for cell reprogramming and early embryonic development in mice. *Nat. Commun.* **9**, 1261 (2018).
72. Sun, X. et al. Loss of RPGR glutamylation underlies the pathogenic mechanism of retinal dystrophy caused by TTLL5 mutations. *Proc. Natl. Acad. Sci. USA* **113**, E2925–E2934 (2016).

73. van Dijk, J. et al. Polyglutamylation is a post-translational modification with a broad range of substrates. *J. Biol. Chem.* **283**, 3915–3922 (2008).
74. Applegate, K. T. et al. plusTipTracker: Quantitative image analysis software for the measurement of microtubule dynamics. *J. Struct. Biol.* **176**, 168–184 (2011).

ACKNOWLEDGEMENTS

We are especially grateful to C. Janke for the gift of antibodies and plasmids and advice about polyglutamylation experiments and reagents. We thank NYULH DART Microscopy Laboratory Chris Petzold, Yan Deng and Kristen Dancel-Manning for assistance with CLEM work, and this core is partially funded by NYU Cancer Center Support Grant NIH/NCI P30CA016087. We thank B. Ueberheide and the NYU Langone's Proteomics Laboratory for assistance with MS analysis. The Proteomics Laboratory is supported in part by NYU Langone Health and the Laura and Isaac Perlmutter Cancer Center support grant P30CA016087 from the National Cancer Institute. The content is solely the responsibility of the authors and does not necessarily represent the official views of the National Center for Research Resources or the National Institutes of Health. We thank D.-S. Lim, J. Kim, Y. Lin, J. I. Cheeseman, K. Ikegami, S. Mitsutoshi and A. Lennon-Duménil for the generous gifts of plasmids and antibodies detailed in Materials and methods. Work in H. Knaut's laboratory was supported by R01NS102322. Work in BDD's laboratory was supported by 9R01GM120776 and a DOD prostate cancer postdoctoral training award W81XWH-16-1-0392 to L.W.

AUTHOR CONTRIBUTIONS

L.W. and B.D.D. designed the experiments, and L.W. conducted the experiments. L.W., B.D.D., and I.S. contributed to the generation of CRISPR KO cells. S.C.P. and A.S. contributed to the nuclear shape, nuclear MT analysis, and MT polyglutamylation analysis. Y.K. contributed to the cilia disassembly analysis. M.O. provided reagents and performed the flow cytometry analysis. F.-X.L. assisted with CLEM and analysis of EM data. H.K. helped with the zebrafish study. I.S. generated constructs and assisted with biochemistry analysis. L.W. and B.D.D. analyzed the data and wrote the manuscript, and all authors were involved in reading and correcting the manuscript.

COMPETING INTERESTS

The authors declare no competing interests.

ADDITIONAL INFORMATION

Supplementary information The online version contains supplementary material available at https://doi.org/10.1038/s41422-021-00584-9.

Correspondence and requests for materials should be addressed to Lei Wang or Brian D. Dynlacht.